

Sensor and Simulation Notes

Note 129

May 1971

Geometrical Diffraction Solution for the High Frequency-Early
Time Behavior of the Field Radiated by an Infinite
Cylindrical Antenna With a Biconical Feed

by

M. I. Sancer and A. D. Varvatsis
Northrop Corporate Laboratories
Pasadena, California

Abstract

In this note we study the high frequency diffraction due to the junction between the biconical wave launcher and the cylindrical portion of the antenna. We also study the early time breaking effect on the radiated electromagnetic pulse due to this junction. The high frequency solution is obtained by employing the geometrical theory of diffraction and then the early time solution is derived by taking the inverse Fourier transform of the diffraction solution. We obtain early time diffraction coefficients corresponding to each of the junctions where the bicone joins the cylinder. These coefficients are compared to those that appear in a previous note.

CLEARED
FOR PUBLIC RELEASE

PL/PA 7 JAN 97

PL 96-1171

I. Introduction

A method for achieving the desired early time behavior of a pulse-radiating dipole antenna is to employ a biconical feeding section^[1]. This system is depicted in figure 1. In this note we investigate the effect on the radiated pulse of the edge formed by the joining of the bicone to the cylindrical portion of the antenna. Since we are interested in the diffraction effect of an edge at high frequencies, it is reasonable to employ the geometrical theory of diffraction^{[2],[3]}. This method yields high-frequency corrections to the geometric optics solution. A quantitative error bound has not been established for solutions obtained by this method; however, numerous comparisons between exact and experimental results with geometrical diffraction solutions have supported its validity. Eventhough the high frequency solution itself is of interest, our primary interest is in the early time solution which exhibits the effect of the edge on a pulse. We obtain our early time solution by taking the inverse Fourier transform of the geometrical diffraction solution. A quantitative validity time for which such a solution is a good approximation can not be determined. There is no way of determining this time duration even if we knew that the geometrical diffraction method gave the exact high frequency asymptotic solution; however, in appendix A we establish that there is a finite length of time for which the asymptotic solution obtained by this method is a good approximation to the exact solution. In that appendix we compare the approximate and exact solutions for the problem of scattering by a perfectly conducting wedge.

We believe that this procedure yields a good approximation to the exact early time asymptotic solution and that it accurately predicts the breaking effect of the edge for a short but finite length of time. The form of the solution is a quite tractable function of the bicone angle, the radius of the cylinder, and the observation angle. Because of this, one can readily study the edge breaking effect as a function of these variables.

The problem studied in this note was also studied by Barnes^[4] by a method we will refer to as the aperture integration method. In appendix B we again study the problem of scattering by a perfectly conducting wedge by the aperture integration method. It is found that the aperture integration

method yields a good approximation to the exact solution for an extended period of time; however, our method yields the exact early time asymptotic solution. This study also supported Baum's contention (private communication) that the exact solution is always larger than the one obtained by the aperture integration method. Our contribution to the time dependent solution of this pulse radiating antenna is the prediction of the diffraction coefficients which describe the breaking effect of both the upper and lower edge on the pulse radiated by this antenna. We present tables and curves which summarize these early time diffraction coefficients. In the tables we also present Barnes's coefficients and in our set of curves we plot a ratio that indicates the percentage difference between our coefficients and those of Barnes. This ratio is small corresponding to the break from the upper edge, but is appreciable for the second break corresponding to the lower edge.

III. Pertinent Aspects of Geometrical Diffraction Theory

Those aspects of the geometrical theory of diffraction which are used in our problem are the following:

1. A wave is any quantity that satisfies a Helmholtz equation, scalar or vector, and it can be expressed as

$$\underline{U} = \underline{A}(\underline{r}) \exp[ik\psi(\underline{r})] \quad (1)$$

In our problem \underline{U} will be the magnetic field and \underline{A} will be a vector.

2. Rays are the orthogonal trajectories to the wave fronts $\psi(\underline{r}) = \text{constant}$.
3. The field at any point in space is the sum of the fields associated with the rays passing through that point. The phase of the field on a ray is assumed to be k times the optical length of the ray measured from some reference point, where the phase is zero, to the observation point. The amplitude is assumed to vary in accordance with the principle of conservation of energy in a narrow tube of rays. The direction of \underline{A} is perpendicular to the ray and in a homogeneous medium this vector slides parallel to itself along the ray. Finally, in such a medium all rays are straight lines.

The preceding three numbered statements have been extensively used in ordinary geometrical optics. A significant statement in the geometrical theory of diffraction is that these same rules can be used to assign a field to each diffracted ray. For our problem a diffracted ray is one that is produced when an incident ray hits an edge. When applying this theory to edge diffracted rays, one must answer the following two questions. Into what direction can an incident ray be diffracted? What "coefficient" should the field on an incident ray be multiplied by in order to describe the initial behavior of the field on a diffracted ray. For the vector case of interest, this "coefficient" is a matrix. Both of these questions will be answered as we discuss our particular geometry.

III. The Direction of the Diffracted Rays

Consider the geometry depicted in figure 1. The antenna of interest is the one obtained by imagining the figure to be rotated about the z axis. The jagged lines are used to indicate that the antenna extends between z tending to $\pm\infty$. The surface at $r = b$ corresponds to our source and we consider that the electric field is specified on this surface in such a way that it corresponds to the electric field of the TEM mode of an infinite biconical antenna. In this note we assume that b is vanishingly small. With this source the magnetic field that is generated is the TEM magnetic field and this is used to define the field incident on the upper and lower edges, P_U and P_L . Our problem is ϕ independent so we chose $\phi = 0$ in figure 1. The rules governing diffracted rays are such that for our problem all diffracted rays will remain in the $\phi = 0$ plane. Shortly this rule will be given in more detail. If our observation point P lies in this plane then it is only those rays associated with the incident magnetic field that lie in this plane that can be diffracted into the direction that allows them to pass through P . For the TEM magnetic field, the associated rays are all radially directed and consequently they strike the junction between the bicone and cylinder at a right angle. The general rule for determining the direction of the diffracted rays for this angle of incidence is as follows. Imagine a plane that contains the incident ray and that has as its normal the vector that is tangent to the edge at the point of incidence. All diffracted rays will lie in this plane and they will be radial lines with their origin at the point of incidence. When the angle of incidence is other than 90° a more general rule for determining the direction of the diffracted rays is necessary. Since it is not pertinent to our problem we will not state it in this note; however, it can be found in reference 3. Referring back to figure 1 we can trace out the path that diffracted rays must take in order to pass through P . The ray associated with $H_1(P_U)$ strikes the edge at P_U and gets initially diffracted into four directions that could allow a diffracted ray to pass through P . The ray we first consider is the one associated with H_1 . This ray is the one that is directly diffracted into a direction that causes it to pass through P and the corresponding field, H_1 , will be seen to decrease the most slowly with increasing frequency of all those

diffracted fields associated with P_U . The frequency dependence of any singly diffracted ray is $k^{-1/2}$ times the incident field. A second direction that allows a ray to pass through P is along the straight line from P_U to P_L . After it strikes P_L it can be diffracted so as to pass through P. The field associated with this double diffracted ray just discussed is \underline{H}_3 . We can now see that the ray directed from P_U to P_L can initiate an infinite number of rays that pass through P. For example the next case is that of the triply diffracted ray traveling from P_U to P_L to P_U to P. The third direction to be considered for the initial diffraction at P_U is back toward our source surface S_b . The uncertainty of how to handle the contribution to the total field due to this ray places a limitation on our analysis. We may handle this in either of two ways. One is to calculate the time, t_c , that this contribution would arrive at our observation point and to state that our solution could have validity at most up to this time. Another possibility is to assume that the source is designed to absorb the field associated with this ray and its effect is never felt at P. The fourth direction we consider is from P_U onto the walls of the bicone so that the diffracted ray can be reflected so as to pass through P. This effect is indicated by \underline{H}_R and is treated in detail in the appendix. To summarize, the diffracted field that passes through P initially started at P_U and was directly diffracted to P, multiply diffracted to P, or singly or multiply diffracted and then reflected to P. Clearly the same discussion applies for the ray that is initially diffracted at P_L .

IV. High Frequency Diffraction Field Calculation

First we attach right handed coordinates (T_U, N_U, B_U) and (T_L, N_L, B_L) at P_U and P_L (see figure 2). We will resolve our incident magnetic field into these coordinates. This field is given by

$$H_i(P_U) = H_i(P_L) = h \hat{a}_\phi \quad (2)$$

where

$$h = \frac{V(\omega) f_o e^{ikd}}{2d \sin \theta_o Z_o} \quad (3)$$

$$f_o = \{2 \ln[\cot(\theta_o/2)]\}^{-1} \quad (4)$$

$$d = \sqrt{L^2 + a^2} \quad (5)$$

$$Z_o = \sqrt{\mu_o/\epsilon_o}, \quad k = \omega \sqrt{\mu_o \epsilon_o} \quad (6)$$

and $V(\omega)$ is the voltage difference between the two cones as measured along a radial arc. It should be noted that h is one half of the TEM bicone field rather than the total field. The reason for this half factor is that the entire TEM bicone field is equally divided between the incident field and the reflected field and it is only the incident field that enters into this calculation.

We now note that $\hat{T}_U = -\hat{a}_\phi$ and $\hat{T}_L = \hat{a}_\phi$. For this reason we resolve the incident field on P_U as follows

$$\underline{H}_i(P_U) = -h \hat{T}_U \quad (7)$$

and

$$\underline{H}_i(P_L) = h \hat{T}_L \quad (8)$$

We are now ready to obtain the singly diffracted fields that pass through P. The field coming directly from P_U is

$$\underline{H}_1 = A(\delta_1, s_1) f(s_1) k^{-1/2} \underline{D}_{\underline{U}}(\alpha_1, \beta_1, \gamma_1) \cdot \underline{H}_i(P_U) \quad (9)$$

where

$$A(\delta, s) = |1 - (s/a) \cos \delta|^{-1/2} \quad (10)$$

$$f(s) = s^{-1/2} e^{iks} \quad (11)$$

$$\underline{D}_{\underline{U}} = \underline{B} \underline{W}_{\underline{U}} \quad (12)$$

$$B = \frac{\lambda \sin \lambda \pi}{\sqrt{2\pi}} e^{i\pi/4} \quad (13)$$

$$\lambda = (1 + \theta_o/\pi)^{-1} \quad (14)$$

$$\underline{W}_{\underline{U}} = \begin{bmatrix} U + V & 0 & 0 \\ (U + V) \cot \gamma \sin \beta & -(U - V) \cos \alpha \cos \beta & (U - V) \sin \alpha \cos \beta \\ (U + V) \cot \gamma \cos \beta & (U - V) \cos \alpha \sin \beta & -(U - V) \sin \alpha \sin \beta \end{bmatrix} \quad (15)$$

$$U = (\cos \lambda \pi - \cos \lambda(\pi - \beta + \alpha))^{-1} \quad (16)$$

$$V = (\cos \lambda \pi + \cos \lambda(\pi - \beta - \alpha))^{-1} \quad (17)$$

The dyadic \underline{D} is obtained by solving the canonical wedge problem. We obtained this quantity by slightly modifying the dyadic for an electric field geometric diffraction analysis contained in a recent paper by Senior and Uslenghi^[5].

The remaining factors $Afk^{-\frac{1}{2}}$ are well known [3]. The calculation of A can sometimes be very difficult; however, because of the symmetry of our excitation and of the bicone this quantity was comparatively easy to obtain since our diffraction caustic was always the axis of the cylinder. For a more detailed discussion of A see reference 3. The ordering of the rows and columns in \underline{W}_U is $\hat{T}_U, \hat{N}_U, \hat{B}_U$. The angle between the incident ray and the negative B_U axis is α_1 and the angle between this axis and the line joining P_U and P is β_1 . The angle between this line and Δ_U is δ_1 . The length of this line is s_1 . These quantities are depicted in figure 2. The angle γ_1 is between the tangent to the edge at P_U and the incident ray. Explicitly these factors are

$$s_1 = (r^2 + d^2 - 2r(a \sin \theta + L \cos \theta))^{\frac{1}{2}} \quad (18)$$

$$\alpha_1 = \pi - \Omega \quad (19)$$

$$\beta_1 = \Omega + \xi_1 \quad (20)$$

$$\xi_1 = \begin{cases} \pi - \arctan\left(\frac{r \sin \theta - a}{L - r \cos \theta}\right) & L > r \cos \theta \\ \arctan\left(\frac{r \sin \theta - a}{r \cos \theta - L}\right) & r \cos \theta > L \end{cases} \quad (21)$$

$$\delta_1 = \frac{\pi}{2} + \tau_1 \quad (22)$$

$$\tau_1 = \arctan\left(\frac{r \sin \theta - a}{|L - r \cos \theta|}\right) \quad (23)$$

$$\gamma_1 = \frac{\pi}{2} \quad (24)$$

$$\Omega = \frac{\pi - \theta_0}{2} \quad (25)$$

Similarly the singly diffracted ray from P_L is

$$\underline{H}_2 = A(\delta_2, s_2) f(s_2) k^{-\frac{1}{2}} \underline{D}_L(\alpha_2, \beta_2, \gamma_2) \cdot \underline{H}_1(P_L) \quad (26)$$

where A and f are defined in (11) and (12). \underline{D}_L has the same definition as \underline{D}_U except now the rows and columns are associated with $\hat{T}_L, \hat{N}_L, \hat{E}_L$. The angles α_2 and β_2 are measured with respect to the negative B_L axis and δ_2 is measured from the A_L axis. Explicitly these quantities are

$$s_2 = (r^2 + d^2 + 2r(L \cos \theta - a \sin \theta))^{\frac{1}{2}} \quad (27)$$

$$\alpha_2 = \pi - \Omega = \alpha_1 \quad (28)$$

$$\beta_2 = \Omega + \frac{\pi}{2} + \xi_2 \quad (29)$$

$$\delta_2 = \pi - \xi_2 \quad (30)$$

$$\xi_2 = \arctan\left(\frac{L+r \cos \theta}{r \sin \theta - a}\right) \quad (31)$$

$$\gamma_2 = \frac{\pi}{2} \quad (32)$$

We now consider the field diffracted from P_U to P_L to P. First we consider the diffraction from P_U to P_L and having direction \hat{T}_L . It is

$$\underline{H}'_i(P_L) = A(\delta_3, s_3) f(s_3) k^{-\frac{1}{2}} \underline{D}_U(\alpha_3, \beta_3, \gamma_3) \cdot \underline{H}_i(P_U) \quad (33)$$

and this is in the $-\hat{T}_L$ direction. We introduce the subscript i because the diffracted ray is now an incident ray on P_L . The arguments of the quantities that appear in (33) are

$$\delta_3 = \pi/2, s_3 = 2L, \alpha_3 = \alpha_1, \beta_3 = \Omega + \pi, \gamma_3 = \pi/2 \quad (34)$$

Now to go from P_L to P we can use (26) with $\underline{H}_1(P_L)$ replaced by $-\underline{H}_1(P_L)$ and α_2 replaced by Ω . Explicitly

$$\underline{H}_3 = A(\delta_2, s_2) f(s_2) k^{-\frac{1}{2}} \underline{D}_{\underline{L}}(\Omega, \beta_2, \pi/2) \cdot [-A(\delta_3, s_3) f(s_3) k^{-\frac{1}{2}} \underline{D}_{\underline{U}}(\alpha_3, \beta_3, \gamma_3) \cdot \underline{H}_1(P_U)] \quad (35)$$

It should be noted that \underline{H}_3 is the first doubly diffracted field we consider and it is $O(k^{-1})$. To obtain the field diffracted from P_L to P_U to P we first consider the diffraction from P_L to P_U . This is given by

$$\underline{H}'_1(P_U) = A(\delta_4, s_4) f(s_4) k^{-\frac{1}{2}} \underline{D}_{\underline{L}}(\alpha_4, \beta_4, \gamma_4) \cdot \underline{H}_1(P_L) \quad (36)$$

and this is in the $-\hat{T}_U$ direction. The arguments that appear in (36) are

$$\delta_4 = \pi/2, s_4 = 2L, \alpha_4 = \alpha_2 = \alpha_1, \beta_4 = \Omega + \pi, \gamma_4 = \pi/2 \quad (37)$$

As before the field then rediffracted to P is

$$\underline{H}_4 = A(\delta_1, s_1) f(s_1) k^{-\frac{1}{2}} \underline{D}_{\underline{U}}(\Omega, \beta_1, \gamma_1) \cdot [-A(\delta_4, s_4) f(s_4) k^{-\frac{1}{2}} \underline{D}_{\underline{L}}(\alpha_4, \beta_4, \gamma_4) \cdot \underline{H}_1(P_L)] \quad (38)$$

Now there are a set of rays that are best discussed for a particular geometry. These are the rays corresponding to a diffraction and a reflection before they pass through P . We will now present the fields corresponding to these rays for a special case that was also treated by Barnes^[4] in detail. That case corresponds to $a = 5$ meters and $L = 10$ meters so that $\theta_0 = \arctan \frac{1}{2}$, $0 < \theta \leq \pi/2$, and it is necessary that the diffracted ray start from P_L , strike the upper cone and then get reflected to P . The singly diffracted and reflected contribution is

$$\underline{H}_5 = A(\delta_5, s_5) f(s_5) k^{-\frac{1}{2}} \underline{D}_{\underline{L}}(\alpha_2, \beta_5, \pi/2) \cdot \underline{H}_1(P_L) \quad (39)$$

and the doubly diffracted and then reflected contribution

$$\underline{H}_6 = A(\delta_5, s_5) f(s_5) k^{-\frac{1}{2}} \underline{D}_{\underline{L}}(\Omega, \beta_5, \pi/2) \cdot [-\underline{H}'_1(P_L)] \quad (40)$$

where $\underline{H}_1(P_L)$ is given in (33). The determination of δ_5, s_5 , and β_5 appears in the appendix. They are

$$\delta_5 = \pi/2 + \psi - \theta_0, \quad \beta_5 = 2\pi - \Omega - \psi \quad (41)$$

where

$$\psi = \arccos\left(\frac{d+r \cos(3\theta_0 - \theta)}{s_5}\right) \quad (42)$$

$$s_5 = (r^2 + d^2 + 2rd \cos(3\theta_0 - \theta))^{1/2} \quad (43)$$

In the appendix it is also shown that \underline{H}_5 and \underline{H}_6 contribute to the total diffracted field if the observation angle θ lies between θ_1 and θ_2 where they are given by

$$\theta_1 = \arccos \frac{L + ((r^2 - L^2)^{1/2} - a) \cos 2\theta_0}{r} \quad (44)$$

and

$$\theta_2 = 3\theta_0 \quad (45)$$

For this reason we introduce the function $P(\theta_1, \theta_2)$ given by

$$P(\theta_1, \theta_2) = U(\theta - \theta_1) - U(\theta - \theta_2) \quad (46)$$

where U is the unit step function. Finally, the total diffracted field through $O(k^{-1})$ is

$$\underline{H}_D = \underline{H}_D \hat{a}_\phi = -\underline{H}_1 + \underline{H}_2 + \underline{H}_3 - \underline{H}_4 + P(\theta_1, \theta_2)(\underline{H}_5 + \underline{H}_6) \quad (47)$$

The negative signs in front of \underline{H}_1 and \underline{H}_4 are due to the fact that the final dyadic multiplication involved \underline{D}_U and $\hat{T}_U = -\hat{a}_\phi$. It should be noted that all of the terms on the right hand side of (47) are directed along \hat{a}_ϕ . The only components of \underline{D}_U and \underline{D}_L which were used in obtaining (47) were $(U + V)\hat{T}_U\hat{T}_U$ and $(U + V)\hat{T}_L\hat{T}_L$. It might appear that the vector nature of our calculation

was superfluous since only the ϕ component of the magnetic field was ever involved in our calculation. It was necessary to treat vector magnetic fields rather than only the ϕ component since $h_{\phi} \hat{a}_{\phi}$ satisfies a vector wave equation but h_{ϕ} does not satisfy a scalar wave equation. We are interested in $E_{\theta D}$ and we obtain it from H_D through

$$\nabla \times H_D \hat{a}_{\phi} = -i\omega \epsilon_0 E_{\theta D} \quad (48)$$

which implies

$$i\omega \epsilon_0 E_{\theta D} = \frac{\partial H_D}{\partial r} + \frac{1}{r} H_D \quad (49)$$

In order to calculate $E_{\theta D}$ to only as high an order in inverse powers of $k^{\frac{1}{2}}$ as we are permitted in order to be consistent with our calculation of H_D we will consider only part of the radial derivative term in the right hand side of (49). That is

$$\frac{\partial}{\partial r} f(s_i) = ikf(s_i) \frac{\partial s_i}{\partial r} - \frac{1}{2s_i} f(s_i) \quad (50)$$

and it is only the first term on the right hand side of (50) that can be used in computing $\partial H_D / \partial r$. This leads to

$$E_{\theta D} = Z_0 \left[-H_1 \frac{\partial s_1}{\partial r} + H_2 \frac{\partial s_2}{\partial r} + H_3 \frac{\partial s_2}{\partial r} - H_2 \frac{\partial s_1}{\partial r} + P(\theta_1, \theta_2) \left[H_5 \frac{\partial s_5}{\partial r} + H_6 \frac{\partial s_6}{\partial r} \right] \right] \quad (51)$$

where

$$\frac{\partial s_1}{\partial r} = \frac{r - (a \sin \theta + L \cos \theta)}{s_1} \quad (52)$$

$$\frac{\partial s_2}{\partial r} = \frac{r + L \cos \theta - a \sin \theta}{s_2} \quad (53)$$

$$\frac{\partial s_5}{\partial r} = \frac{r + d \cos(3\theta_0 - \theta)}{s_5} \quad (54)$$

Combining our results we obtain

$$\begin{aligned}
 E_{\theta D} = & \frac{V(\omega) f_0 e^{ikd}}{2d \sin \theta_0} B \left\{ A(\delta_1, s_1) g(\alpha_1, \beta_1) (ks_1)^{-\frac{1}{2}} e^{iks_1} \frac{\partial s_1}{\partial r} \right. \\
 & + A(\delta_2, s_2) g(\alpha_1, \beta_2) (ks_2)^{-\frac{1}{2}} e^{iks_2} \frac{\partial s_2}{\partial r} \\
 & + Bg(\alpha_1, \Omega + \pi) A(\delta_2, s_2) g(\Omega, \beta_2) (2Ls_2)^{-\frac{1}{2}} k^{-1} e^{ik2L} e^{iks_2} \frac{\partial s_2}{\partial r} \\
 & + Bg(\alpha_1, \Omega + \pi) A(\delta_1, s_1) g(\Omega, \beta_1) (2Ls_1)^{-\frac{1}{2}} k^{-1} e^{ik2L} e^{iks_1} \frac{\partial s_1}{\partial r} \\
 & + P(\theta_1, \theta_2) \frac{\partial s_5}{\partial r} e^{iks_5} A(\delta_5, s_r) \\
 & \left. \times [g(\alpha_1, \beta_5) (ks_5)^{-\frac{1}{2}} + g(\alpha_1, \Omega + \pi) g(\Omega, \beta_5) (2Ls_5)^{-\frac{1}{2}} k^{-1} e^{ik2L}] \right\} \quad (55)
 \end{aligned}$$

where for convenience

$$g(\alpha, \beta) = U + V \quad (56)$$

with U and V defined in (16) and (17). Equation (55) is the final expression for $E_{\theta D}$ for a calculation through $O(k^{-1})$.

The quantitative validity of (55) has not been established. Even if we know that (55) is the correct asymptotic expansion through $O(k^{-1})$ we could draw no conclusions concerning the length of time the inverse Fourier transform of (55) is a good approximation. We determine an upper bound in the region $\pi/2 \geq \theta > \theta_0$ by comparing our results with those of Barnes^[4]. We believe that the exact solution is always larger than that obtained by Barnes and the time at which the inverse Fourier transform crosses Barnes solution is the maximum validity time for the solution obtained by the method employed in this note. The general argument concerning Barnes's solution being lower

than the exact solution was supplied by Baum (private communication). Briefly it is that if the appropriate Green's function is used, then the exact radiated field can be expressed as the integral over the cylindrical aperture used in Barnes's note. The exact radiated field would be obtained if the exact aperture electric field were employed; however, Barnes employs only the incident electric field. It is argued that the exact aperture field is larger than the incident field so that the exact radiated field is larger than the one calculated by Barnes. There are some subtleties that could be studied concerning this argument, two in particular, are the occurrence of the time derivative of the aperture field and the constancy of the sign of the time dependent Green's function. It is not possible to perform a precise study of Baum's argument for the bicone problem because we are not positive of how the edge diffraction effects the aperture field. Instead we study the analogous problem in two dimensions where we have the exact wedge solution available. This study is performed in the appendix and it completely supports Baum's argument. Another feature of the wedge study is that eventhough the solution obtained by employing only the incident field in the aperture is always lower than the exact field, the degree of approximation to the radiated field that one obtains is excellent. This observation supports the possibility that the solution obtained by Barnes might have an extensive range of time for which it is an excellent approximation. Our contribution to the time dependent bicone solution is for very short times after the breaking effect of the edge is felt at the observation point. In the next section we will determine the early time asymptotic solution which describes the breaking effect.

V. Early Time Asymptotic Solution

To determine the most reliable early time asymptotic solution we consider the inverse Fourier transform of only the first term in (55) or for the special observation angle $\theta = \pi/2$ the first two terms in (55). It is first necessary to specify the form of $V(\omega)$. We are interested in the case $V(t) = V_{bo} U(t)$, where $U(t)$ is the unit step. For this case

$$V(\omega) = V_{bo} \frac{1}{\omega} \quad (57)$$

We need only consider the inverse Fourier transform

$$F^{-1}(k^{-1/2} \frac{1}{\omega} e^{iks}) = c^{1/2} e^{-i\pi/4} \frac{2}{\sqrt{\pi}} \sqrt{t - \frac{s}{c}} U(t - \frac{s}{c}) \quad (58)$$

where c is the speed of light. We now take the inverse transform of these two terms to obtain

$$E_{\theta D} \sim \frac{f_o V_{bo} Q}{2a} \left\{ \left(\frac{c_1}{s_1} \right)^{1/2} \frac{2}{\sqrt{\pi}} (t^* - t_1)^{1/2} U(t^* - t_1) A(\delta_1, s_1) g(\alpha_1, \beta_1) \frac{\partial s_1}{\partial r} \right. \\ \left. + \left(\frac{c_1}{s_2} \right)^{1/2} \frac{2}{\sqrt{\pi}} (t^* - t_2)^{1/2} U(t^* - t_2) A(\delta_2, s_2) g(\alpha_1, \beta_2) \frac{\partial s_2}{\partial r} \right\} \quad (59)$$

where

$$Q = \frac{\lambda \sin \lambda \pi}{\sqrt{2\pi}}, \quad c_1 = c \times 10^{-9}, \quad t^* = 10^9 (t - \frac{r}{c}) \quad (60)$$

The physical meaning of these t 's will now be discussed. The time after the first signal arrives from the origin measured in nanoseconds is t^* . When t^* equals t_1 and t_2 the corresponding contributions arise from single diffraction from P_U and P_L .

In order to compare our results with those of Barnes^[4] we approximate (59) for the case $r \gg d$. When this is the case we obtain the following simplifications

$\beta_1 \approx \Omega + \theta$, $\beta_2 \approx \Omega + \pi - \theta$, $\delta_1 \approx \delta_2 \approx \pi/2 + \theta$

$$A(\delta_1, s_1) \approx A(\delta_2, s_2) \approx [(r/a) \sin \theta]^{-1/2}, \quad (61)$$

$$c_1 t_1 = d - a \sin \theta - L \cos \theta, \quad c_1 t_2 = d - a \sin \theta + L \cos \theta$$

and when the following quantities appear as multiplicative factors they are approximated as

$$(s_1)^{-1/2} \approx (s_2)^{-1/2} \approx r^{-1/2}, \quad \frac{\partial s_1}{\partial r} \approx \frac{\partial s_2}{\partial r} \approx 1. \quad (62)$$

Using the fact that the geometric optics field is

$$E_{\theta G.O.} = P[\theta_0, \frac{\pi}{2}] \frac{V_{bo} f_o}{r \sin \theta} U(t^*) \quad (63)$$

we can express the total field $E_\theta = E_{\theta D} + E_{\theta G.O.}$ so that

$$rE_\theta \sim rE_1 + rE_2 \quad (64)$$

where

$$rE_1 = \frac{V_{bo} f_o}{\sin \theta} \left[P(\theta_0, \frac{\pi}{2}) + Q\left(\frac{c_1 \sin \theta}{\pi a}\right)^{1/2} g(\alpha_1, \beta_1) (t^* - t_1)^{1/2} U(t^* - t_1) \right] \quad (65)$$

and

$$rE_2 = \frac{V_{bo} f_o}{\sin \theta} Q\left(\frac{c_1 \sin \theta}{\pi a}\right)^{1/2} g(\alpha_1, \beta_2) (t^* - t_2)^{1/2} U(t^* - t_2) \quad (66)$$

When $\theta \neq \pi/2$ then $E_\theta \sim E_1$. When $\theta = \pi/2$, then $t_1 = t_2$ and $g(\alpha_1, \beta_1) = g(\alpha_1, \beta_2) = g(\alpha_1, \Omega + \pi/2)$ so that

$$rE_\theta \sim V_{bo} f_o \left[1 + 2Q\left(\frac{c_1}{\pi a}\right)^{1/2} g(\alpha_1, \Omega + \frac{\pi}{2}) (t^* - t_1)^{1/2} U(t^* - t_1) \right] \quad (67)$$

It is desired to compare (65), (66) and (67) with the solution obtained by Barnes. It is convenient to rewrite these equations as

$$rE_1 = \frac{V_{bo} f_o}{\sin \theta} \left[P(\theta_o, \frac{\pi}{2}) - \frac{1}{\pi} \left(\frac{2c_1 \sin \theta}{a} \right)^{\frac{1}{2}} A_1(\theta_o, \theta) (t^* - t_1)^{\frac{1}{2}} U(t^* - t_1) \right] \quad (68)$$

$$rE_2 = - \frac{V_{bo} f_o}{\pi \sin \theta} \left(\frac{2c_1 \sin \theta}{a} \right)^{\frac{1}{2}} A_2(\theta_o, \theta) (t^* - t_2)^{\frac{1}{2}} U(t^* - t_2) \quad (69)$$

and for $\theta = \pi/2$

$$rE_\theta \sim V_{bo} f_o \left[1 - \frac{2}{\pi} \left(\frac{2c_1}{a} \right)^{\frac{1}{2}} A_1(\theta_o, \frac{\pi}{2}) (t^* - t_1)^{\frac{1}{2}} U(t^* - t_1) \right] \quad (70)$$

where

$$A_1(\theta_o, \theta) = \frac{\lambda \sin \lambda \theta_o}{\cos \lambda \theta_o - \cos \lambda \theta} \quad (71)$$

$$A_2(\theta_o, \theta) = \frac{\lambda \sin \lambda \theta_o}{\cos \lambda \theta_o - \cos \lambda (\pi - \theta)} \quad (72)$$

$$\lambda = \left(1 + \frac{\theta_o}{\pi} \right)^{-1} \quad (73)$$

The corresponding expressions derived by Barnes are exactly the same as (68), (69) and (70) with $A_1(\theta_o, \theta)$ replaced by $B_1(\theta_o, \theta)$ and $A_2(\theta_o, \theta)$ replaced by $B_2(\theta_o, \theta)$ where

$$B_1(\theta_o, \theta) = \frac{\sin \theta_o}{\cos \theta_o - \cos \theta} \quad (74)$$

and

$$B_2(\theta_o, \theta) = \frac{\sin \theta_o}{\cos \theta_o + \cos \theta} \quad (75)$$

It is very important to note that for $\pi/2 \geq \theta > \theta_o$, $B_1(\theta_o, \theta) > A_1(\theta_o, \theta)$, while for $0 < \theta < \theta_o$, $|A_1(\theta_o, \theta)| > |B_1(\theta_o, \theta)|$. This shows that our solution is initially larger than the one obtained by Barnes, as required. For the special

case that was treated in detail by Barnes, $a = 5$ meters and $\theta_0 = \arctan .5$, we can gain some additional information about the length of time our asymptotic solution could be a good approximation. For this case we can see when our asymptotic solution crosses Barnes total solution. For the observation angle, θ , equal to $.7 \pi/2$ we drop below this solution in approximately 1 nanosecond and for $\theta = \pi/2$ we drop below his solution in approximately 3 nanoseconds. For $\theta = .1\pi$ we are always above Barnes's total solution so it imposes no time limitation. It is expected that the difference between $A_1(\theta_0, \theta)$ and $B_1(\theta_0, \theta)$ is monotonically related to the length of time that it would take our solution to cross Barnes's total solution in the region $\pi/2 \geq \theta > \theta_0$. For many cases our asymptotic solution will drop below Barnes's solution before $t^* = t_2$. The reason that we present the asymptotic solution that begins at t_2 is that the breaking effect predicted by this solution would be valid even though the level at which the break occurs is not accurately determined.

Tables 1 through 4 summarize the breaking effect at t_1 and t_2 as predicted by our theory and that of Barnes. In these tables we present the new quantities D_{A1} , D_{B1} , D_{A2} , and D_{B2} as well as t_1 and t_2 for different values of a , θ_0 , and θ . These new quantities are defined as

$$D_{A1} = \alpha |A_1|, D_{B1} = \alpha |B_1|, D_{A2} = \alpha A_2, D_{B2} = \alpha B_2 \quad (76)$$

where

$$\alpha = \frac{1}{\pi} \left(\frac{2c_1 \sin \theta}{a} \right)^{1/2} \quad (77)$$

and in terms of the D's, (68), (69), and (70) can be equivalently written as

$$rE_1 = \frac{V_{bo} f_o}{\sin \theta} \left[1 - D_{A1} (t^* - t_1)^{1/2} U(t^* - t_1) \right] \quad \frac{\pi}{2} \geq \theta > \theta_0 \quad (78)$$

$$rE_1 = \frac{V_{bo} f_o}{\sin \theta} D_{A1} (t^* - t_1)^{1/2} U(t^* - t_1) \quad 0 < \theta < \theta_0 \quad (79)$$

$$rE_2 = - \frac{V_{bo} f_o}{\sin \theta} D_{A2} (t^* - t_2)^{1/2} U(t^* - t_2) \quad 0 < \theta \leq \frac{\pi}{2} \quad (80)$$

Barnes's corresponding solutions are obtained by replacing D_{A_1} by D_{B_1} and D_{A_2} by D_{B_2} . A schematic plot illustrating the early time breaking effect described by (78), (79), and (80) is contained in figure 3.

In table 5 we tabulate the ratios P_1 and P_2 which are given by

$$P_1 = 2 \left| \frac{A_1 - B_1}{A_1 + B_1} \right| \quad (81)$$

and

$$P_2 = 2 \left| \frac{A_2 - B_2}{A_2 + B_2} \right| \quad (82)$$

These quantities are a measure of the relative correction to the asymptotic solution found by Barnes corresponding to the first break due to the upper edge and the second break due to the lower edge.

Table 1 corresponds to $a = 1$, and it is of special interest. By noting (76) and (77) we see that the value of any D for $a \neq 1$ can be determined from the D corresponding to $a = 1$, simply by multiplying by $a^{-1/2}$. If we rewrite the last two equations in (61) as

$$c_1 t_1 = a(\csc \theta_0 - \sin \theta - \cot \theta_0 \cos \theta) \quad (83)$$

$$c_1 t_2 = a(\csc \theta_0 - \sin \theta + \cot \theta_0 \cos \theta) \quad (84)$$

then we see that the value of t_1 or t_2 for $a \neq 1$ can be obtained by multiplying the appropriate t for $a = 1$ by a . Tables 2, 3, and 4 are included only for convenience. Because the values of the D 's, t_1 , and t_2 for $a = 1$ can readily be used to compute these quantities for any value of a , we plot these quantities in figures 4, 5, 6, 7, and 8. Specifically we plot D_{A_1} , D_{A_2} , P_1 , P_2 , t_1 and t_2 versus the observation angle, θ . Each figure corresponds to a different value of the bicone angle, θ_0 .

VI. Discussion of Results

First we will discuss the validity of our frequency dependent solution expressed in (55). Its accuracy is limited for two reasons. One is that a quantitative error bound has not been established for solutions obtained by geometrical diffraction calculations. A second is that the effect of diffracted rays striking the source region is neglected. The first difficulty is somewhat compensated by the fact that numerous comparisons between exact and experimental results with geometrical diffraction solutions have supported its validity. The second limitation can be handled in either of two ways. One is to examine the source region and determine its effect. The second is most easily viewed in the time domain. It is to determine the time that this secondary source contribution would reach our observation point and let this serve as a time limitation beyond which we discard our solution.

The accuracy of our time dependent solutions (78), (79), and (80) is limited by another consideration. There is no quantitative procedure which determines the time duration that the inverse Fourier transform of a high frequency asymptotic expansion is a good approximation. In appendix A we establish that there is a finite length of time for which such a solution is a good approximation. Because of this our early time asymptotic solution can be used to describe the breaking effect of the edge formed by the junction of the bicone and the cylinder. This early time behavior is described by two coefficients, one corresponding to the junction nearer to the observation point and the other corresponding to the junction further from the observation point. The early time dependent behavior is obtained by multiplying these coefficients by the square root of the time duration beyond the first instant the effect of the junction is felt at the observation point.

The same form for the breaking effect is predicted by Barnes^[4] who uses an aperture integration method. In appendix B we again study the problem of scattering by a perfectly conducting wedge by using the aperture integration method. A comparison of that solution to the exact solution indicates that it can yield a good approximation for an extended time duration; however, the method employed in this paper yields the exact asymptotic solution. In tables 1 through 4 we present our diffraction coefficients as well as those derived by

Barnes. These are presented for both the upper and lower edge and the time that these contributions will first be felt at the observation point is also tabulated. These quantities are presented for different values of the cylinder radius, a , the bicone angle, θ_0 , and the observation angle, θ .

In table 5 we tabulate P_1 and P_2 only for different values of θ and θ_0 because these quantities are independent of a . As previously discussed, by noting (76), (77), (83), and (84) we can see that the data presented in table 1, $a = 1$, can readily be used to compute the D's and t's for any a . In figures 4, 5, 6, 7, and 8 we plot D_{A1} , D_{A2} , P_1 , P_2 , t_1 , and t_2 for $a = 1$. We plot these quantities versus θ and each figure corresponds to a different value of θ_0 . The plot of D_{A1} is cut off near the boundary between the illuminated and diffraction region. The reason for this is that the geometrical diffraction solution diverges at this boundary. It is seen that in general, the percentage difference between our solution and that of Barnes is smaller for the break corresponding to the nearer edge, P_1 , than it is for the break corresponding to the further edge, P_2 . It is also noted that P_1 has a minimum for $\theta = \theta_0$, while P_2 decreases monotonically with increasing θ . Another general feature is that for most observation angles, the break corresponding to the nearer edge is sharper than the break corresponding to the further edge.

In conclusion, the solution obtained by Barnes using the aperture integration method has the potential for being a good approximation for an extended period of time; however, the solution obtained in this note offers an improvement in describing the asymptotic early time breaking effect of the edges, especially from the further edge.

Appendix A. Comparison of the Exact and Approximate Wedge Solutions

Consider a plane wave step function incident on a perfectly conducting wedge with the geometry defined in figure 9. The notation in this appendix was chosen to agree with that used in a previous note that treated the time dependent wedge problem for $\phi_1 = 0$ [6]. The polarization of the incident wave is such that the magnetic field is directed along the positive z axis. For comparison with the singly diffracted bicone problem we can restrict our interest to $\pi/4 < \phi_0 < \pi/2$ and $\phi_1 = \pi - \phi_0$. When $\phi_1 = \pi - \phi_0$ we can write down the solution for the total magnetic field using the work of Keller and Blank [7] as

$$\underline{H} = h \hat{a}_z$$

where

$$h = 1 - \frac{1}{\pi} \arctan \frac{+(1-\rho^{2\lambda}) \cos \lambda(\pi-\phi_1)}{(1+\rho^{2\lambda}) \sin \lambda(\pi-\phi_1) - 2\rho^\lambda \sin \lambda(\pi-\phi)} \quad (A1)$$

$$+ \frac{1}{\pi} \arctan \frac{-(1-\rho^{2\lambda}) \cos \lambda(\pi+\phi_1)}{(1+\rho^{2\lambda}) \sin \lambda(\pi+\phi_1) + 2\rho^\lambda \sin \lambda(\pi-\phi)}$$

and

$$\rho = \left[\frac{ct}{r} + \left(\left(\frac{ct}{r} \right)^2 - 1 \right)^{1/2} \right]^{-1} \quad (A2)$$

$$\lambda = \frac{1}{2} \left(1 - \frac{\phi_0}{\pi} \right)^{-1} \quad (A3)$$

where t is the time after the incident wave hits the tip of the wedge. The arctangent is defined to lie in the range between 0 and π . Actually (A1) is valid for $\phi_0 \leq \phi_1 \leq \pi - \phi_0$. We now compare (A1) with the solution one obtains by taking the inverse Fourier transform of the geometrical diffraction theory solution. For this case the geometrical diffraction solution is precisely the

high frequency asymptotic solution to the wedge diffraction problem. What we are testing in this case is completely a mathematical problem involving the asymptotic properties at high frequencies and early times of an exact Fourier transform pair. It is intended that inferences can be made regarding the early time behavior of electromagnetic problems which are solved by taking the inverse Fourier transform of the geometrical diffraction theory solution when the true time behavior is not known.

In order to present the geometric diffraction solution we consider the incident field slightly bounded away from grazing along the lower portion of the wedge. That is $\phi_1 = \pi - \phi_0 - \epsilon$ and we are interested in the limit as ϵ goes to zero. For this angle of incidence we can, by making a suitable change of coordinates, use the results in reference [8] to express the diffracted field as

$$h_D(\omega) = \frac{\lambda \sin \lambda \pi e^{i\pi/4}}{\sqrt{2\pi k r}} e^{i k r} [(\cos \lambda \pi - \cos \lambda(\pi - \phi + \phi_1))^{-1} + (\cos \lambda \pi + \cos \lambda(\pi - \phi - \phi_1))^{-1}] h_i(\omega) \quad (A4)$$

where $h_i(\omega)$ is the Fourier transform of the incident field evaluated at the tip of the wedge. No matter what the angle of incidence is, the value of $h_i(\omega)$ for an incident plane wave step field is

$$h_i(\omega) = \frac{i}{\omega} \quad (A5)$$

Combining (A4) and (A5) and taking the inverse Fourier transform we obtain

$$h_D(\xi) = \frac{\sqrt{2}}{\pi} \lambda (\sin \lambda \pi) \sqrt{\xi} U(\xi) [(\cos \lambda \pi - \cos \lambda(\pi - \phi + \phi_1))^{-1} + (\cos \lambda \pi + \cos \lambda(\pi - \phi - \phi_1))^{-1}] \quad (A6)$$

where $\xi = (t - r/c)/(r/c)$ and $U(\xi)$ is a Heaviside step function. Physically

ξ is the time after which an observer would first sense the electromagnetic field and it is measured in units of r/c . The total field an observer would sense is either $2 + h_D$ or h_D depending on whether the observer were situated in the illuminated region ($\pi - \phi_0 < \phi < 2\pi - \phi_0$) or in the shadow region ($\phi_0 < \phi < \pi - \phi_0$). We add 2 to the diffracted field rather than 1 to account for the reflected field. Earlier we mentioned that the incident angle was $\pi - \phi_0 - \epsilon$ rather than $\pi - \phi_0$. We did this to emphasize that in using the geometric theory of diffraction it is only the Fourier transform of the incident field, $h_i(\omega)$, which is used in the expression for $h_D(\omega)$. If ϵ were equal to zero then it would appear that the field incident on the tip were $2h_i(\omega)$ rather than $h_i(\omega)$. It is only when we consider the field incident on the tip to be $h_i(\omega)$ that we obtain agreement with the exact solution for high frequencies and early times. We present plots of the approximate magnetic field given by $h_a(\xi) = 2 + h_D(\xi)$ since we are in the illuminated region and of the exact magnetic field $h_e(\xi)$ given by (A1) with

$$\rho = (\xi + 1 + (\xi^2 + 2\xi)^{1/2})^{-1} \quad (A7)$$

A comparison of $h_a(\xi)$ and $h_e(\xi)$ is contained in figures 10 and 11. Figure 10 corresponds to $\phi_0 = 60^\circ$ while figure 11 corresponds to $\phi_0 = 75^\circ$. Both figures contain a comparison of the $h_a(\xi)$ and $h_e(\xi)$ for $\phi = 150^\circ, 165^\circ, 180^\circ$. It is seen that h_a tends to be a better approximation to h_e with increasing ϕ_0 and ϕ .

To relate the wedge and bicone geometries consider figure 12. If we are observing at a distance r such that $r \gg 2L$, then \underline{s} and \underline{r} are approximately parallel and ϕ is related to the bicone observation angle, θ , as $\phi \approx \phi_0 + \theta$. To give a numerical example of the data contained in figures 10 and 11 we consider $\phi_0 = 75^\circ$ and $\theta = 90^\circ$. For this case there is less than a 5% difference between the exact and approximate wedge solutions for $\xi \leq .4$.

Appendix B. Comparison of the Exact Wedge Solution With the One Obtained by Integration Over the Aperture

Consider a perfectly conducting wedge of angle 2Ω with a plane wave pulse propagating parallel to one side of the wedge. The polarization of the incident wave is such that it is parallel to the edge. The geometry is depicted in figure 13.

$$H_{z_{\text{incident}}} = 2U\left(t - \frac{\hat{a} \cdot \rho}{c}\right) = H_{z_i} \quad (\text{B1})$$

where ρ is the two dimensional radius vector and

$$\hat{a} = -[\hat{a}_x \sin \alpha + \hat{a}_y \cos \alpha] \quad (\text{B2})$$

and

$$\alpha = 2\Omega - \frac{\pi}{2} \quad (\text{B3})$$

where t is the time after the field first reaches the edge. In the frequency domain

$$H_{z_i} = \frac{2i}{\omega} e^{ik_0 \hat{a} \cdot \rho} \quad (\text{B4})$$

The analogous approach to that of Barnes^[4] is to represent the magnetic field in the region $y < 0$ as an integral over the plane $y = 0$ and by then reducing this integral so that it is only over the "aperture" or non-conducting portion of this plane. First we write

$$H_z = \int_{S_{\text{aperture}}} \hat{a}_y \cdot [H_z \nabla' G - G \nabla' H_z] dx' + \int_{S_{\text{conductor}}} \hat{a}_y \cdot [H_z \nabla' G - G \nabla' H_z] dx' \quad (\text{B5})$$

and use the fact that

$$\hat{a}_y \cdot \nabla' H_z = -i\omega E_x \quad (B6)$$

as well as a Green's function that has the property

$$\hat{a}_y \cdot \nabla' G = 0 \text{ for } y' = 0 \text{ and } -\infty < x' < \infty \quad (B7)$$

Using (B6) and (B7) in (B5) as well as the fact that $E_x = 0$ for $x' < 0$ we obtain

$$H_z = i\omega \int_{\text{aperture}} dx' E_x G = i\omega \int_0^{\infty} dx' E_x G \quad (B8)$$

The G that satisfies (B7) is

$$G = -\frac{i}{4} \left[H_0^{(1)}(k_0 [(x-x')^2 + (y-y')^2]^{\frac{1}{2}}) + H_0^{(1)}(k_0 [(x-x')^2 + (y+y')^2]^{\frac{1}{2}}) \right] \quad (B9)$$

We now approximate the E_x that appears in (B8) by just the incident field. That is

$$E_x \approx E_{x_i} = Z_0 \cos \alpha H_{z_i} = \cos \alpha \frac{2Z_0 i}{\omega} e^{-ik_0 x' \sin \alpha} \quad (B10)$$

Substituting (B9) and (B10) in (B8) we obtain

$$H_z(\underline{\rho}, \omega) = \int_0^{\infty} dx' H_0^{(1)}(k_0 [(x-x')^2 + y^2]^{\frac{1}{2}}) i \epsilon_0 \cos \alpha Z_0 e^{-ik_0 x' \sin \alpha} \quad (B11)$$

To obtain the time behavior take the inverse Fourier transform

$$H_z(\underline{\rho}, t) = \frac{1}{2\pi} \int_{-\infty}^{\infty} H_z(\underline{\rho}, \omega) e^{-i\omega t} d\omega \quad (B12)$$

Using

$$\frac{1}{2\pi} \int_{-\infty}^{\infty} H_0^{(1)}(k_0 R) e^{-i\omega t} d\omega = \frac{-2i}{\pi} \frac{c}{\sqrt{c^2 t^2 - R^2}} U(ct - R) \quad (B13)$$

we can express (B12) as

$$H_z = \frac{2}{\pi} \cos \alpha \int_0^{\infty} \frac{dx' U(t - (R - x' \sin \alpha)/c)}{(c^2 (t + (x' \sin \alpha)/c)^2 - R^2)^{\frac{1}{2}}} \quad (\text{B14})$$

where

$$R = [(x - x')^2 + y^2]^{\frac{1}{2}} \quad (\text{B15})$$

Equation (B14) could also be derived by substituting the time dependent representation of E_x given in (B10) into a general formula derived in a previous note [9]. The unit step function in (B14) is unity as long as $x_1 < x' < x_2$ where

$$x_1 = (\cos^2 \alpha)^{-1} [T - (T^2 - (\rho^2 - c^2 t^2) \cos^2 \alpha)^{\frac{1}{2}}] \quad (\text{B16a})$$

$$x_2 = (\cos^2 \alpha)^{-1} [T + (T^2 + (\rho^2 - c^2 t^2) \cos^2 \alpha)^{\frac{1}{2}}] \quad (\text{B16b})$$

$$T = x + ct \sin \alpha \quad (\text{B17})$$

After changing variables we can write (B14) as

$$H_z = \frac{2}{\pi} \int_{W_1}^{W_2} \frac{d\xi}{(1 - \xi^2)^{\frac{1}{2}}} \quad (\text{B18})$$

where

$$W_2 = W(x_2), \quad W_1 = W(x_1), \quad W(x) = \frac{x \cos^2 \alpha - T}{(T^2 - (\rho^2 - c^2 t^2) \cos^2 \alpha)^{\frac{1}{2}}} \quad (\text{B19})$$

Equation (B19) is meaningful only if W_2 and W_1 are real, i.e.

$$T^2 - (\rho^2 - c^2 t^2) \cos^2 \alpha > 0 \quad (\text{B20})$$

The smallest value of t that allows (B20) to be satisfied is denoted t_0 and is given by

$$t_0 = \frac{|y| \cos \alpha - x \sin \alpha}{c} \quad (\text{B21})$$

Another critical time occurs when $x_1 = 0$ since for larger t , zero is still the minimum value of x' . The time corresponding to $x_1 = 0$ is denoted by t_1 and it is found to be

$$t_1 = \rho/c \quad (\text{B22})$$

Returning to (B18) we now write

$$H_z = [U(t - t_0) - U(t - t_1)] \frac{2}{\pi} \int_{W_1}^{W_2} \frac{d\xi}{(1-\xi^2)^{1/2}} + U(t - t_1) \frac{2}{\pi} \int_{W(0)}^{W_2} \frac{d\xi}{(1-\xi^2)^{1/2}} \quad (\text{B23})$$

It is easy to verify that $W_1 = -1$, $W_2 = 1$, and

$$W(0) = \frac{-T}{(T^2 - (\rho^2 - c^2 t^2) \cos^2 \alpha)^{1/2}} \quad (\text{B24})$$

In the illuminated region (fig. 5)

$$T > 0 \text{ for } t \geq t_1 \quad (\text{B25})$$

and in the diffraction region

$$T < 0 \text{ for } t_1 \leq t < \frac{|x|}{c \sin \alpha} \text{ and } T \geq 0 \text{ for } \frac{|x|}{c \sin \alpha} \leq t \quad (\text{B26})$$

so finally we have in the illuminated region

$$H_z = 2[U(t - t_0) - U(t - t_1)] + U(t - t_1) \left[1 + \frac{2}{\pi} \arcsin \frac{T}{(T^2 - (\rho^2 - c^2 t^2) \cos^2 \alpha)^{1/2}} \right] \quad (\text{B27})$$

and in the diffraction region

$$H_z = U(t - t_1) \left[1 + \frac{2}{\pi} \arcsin \left(\frac{T}{(T^2 - (\rho^2 - c^2 t^2) \cos^2 \alpha)^{1/2}} \right) \right] \quad (\text{B28})$$

Equations (B27) and (B28) are our final solutions and we will examine them in

the early time and the late time asymptotic limits. Before we do this it is significant to note the functional dependence of the solution expressed in (B27) and (B28) on t , x , and ρ . If we define $ct/\rho = \tau$, redefine a coordinate system so that our z axis corresponds to a new y axis, and define an angle ϕ so that $x = \rho \cos \phi$, then our new H_y for $\tau > 1$ would be a function only of τ and $\cos \phi$. This situation now exactly conforms to the case treated by Baum in a previous note^[9]. When this component has only this functional dependence, he shows how to readily determine all of the remaining field quantities.

We will now refer our wedge geometry to a coordinate system that is more appropriate to the bicone problem. See figure 14. In this coordinate system and for $\theta > \theta_0$ and $t > t_1$ (B27) becomes for early time

$$H_z \sim 2\left(1 - \frac{1}{\pi} \sqrt{\frac{2c}{\rho}} B\tau^{1/2}\right) \quad (B29)$$

$$B = \frac{\sin \theta_0}{\cos \theta_0 - \cos \theta} \quad (B30)$$

$$\tau = t - t_1 \quad (B31)$$

The early time geometric diffraction solution which is necessarily the same as the early time exact solution which is given by

$$H_z \sim 2\left(1 - \frac{1}{\pi} \sqrt{\frac{2c}{\rho}} A\tau^{1/2}\right) \quad (B32)$$

$$A = \frac{\lambda \sin \lambda \theta_0}{\cos \lambda \theta_0 - \cos \lambda \theta} \quad (B33)$$

$$\lambda = \frac{1}{1 + \theta_0/\pi} \quad (B34)$$

Further details concerning the exact solution can be found in references [6] and [7]. It is significant, first, that $A \neq B$ and secondly that in the illuminated region $A < B$. This shows that the field just calculated immediately drops below the true field. In the diffraction region, $\theta < \theta_0$, the approximate solution behaves like

$$H_z \sim \frac{2}{\pi} \sqrt{\frac{2c}{\rho}} |B| \tau^{1/2} \quad (B35)$$

while the exact solution behaves like

$$H_z \sim \frac{2}{\pi} \sqrt{\frac{2c}{\rho}} |A| \tau^{1/2} \quad (B36)$$

and in this region $|A| > |B|$.

For large values of t both the exact and approximate solutions have an asymptotic behavior that is independent of θ and consequently independent of whether or not we are observing in either the illuminated or diffraction region. For large t the approximate solution behaves like

$$H_z \sim 2\left(1 - \frac{\theta}{\pi}\right) \quad (B37)$$

and the exact solution behaves like

$$H_z \sim 2\left(1 - \frac{\theta_0}{\pi}\right) \frac{1}{1 - (\theta_0/\pi)^2} \quad (B38)$$

which is larger for any θ_0 of interest. These results support Baum's claim that the exact solution is always larger than the one obtained by using Barnes's method.

Another interesting result was obtained from doing this test problem. It is that the same factors A and B, which naturally arose in our test problem, also appear in the bicone problem. We expected A to appear simply from the geometric diffraction theory construction; however, the appearance of B from Barnes's asymptotic evaluation of an integral that contained a different Green's function from that of the test problem is an interesting result. Specifically for the bicone problem, Barnes's early time solution can be written as

$$rE_\theta \sim \frac{V_{bo} f_0}{\sin \theta} \left[1 - \frac{1}{\pi} \left(\frac{2c \sin \theta}{a} \right)^{1/2} B \tau^{1/2} U(\tau) \right] \quad \theta > \theta_0 \quad (B39)$$

and

$$rE_{\theta} \sim V_{bo} f_o \frac{1}{\pi} \left(\frac{2c}{a \sin \theta} \right)^{\frac{1}{2}} |B| \tau^{\frac{1}{2}} U(\tau) \quad \theta < \theta_o \quad (B40)$$

where τ is the time after the first diffraction effect is felt. The geometric diffraction solution is the same as (B39) and (B40) with B replaced by A.

Appendix C. Geometrical Considerations for Reflected Rays

In figure 15 we depict that part of the bicone that is necessary to discuss the mechanism which allows rays to be singly or multiply diffracted and then reflected so as to pass through P. Whether or not we are concerned with singly or multiply diffracted rays is immaterial to the analysis contained in this section. Once the edge at P_U or P_L is struck by an incident ray, which may itself be a diffracted ray, then P_U and P_L act as sources for diffracted rays. Figure 15 corresponds to a constant ϕ plane; however, for our geometrical considerations we can imagine that the geometry in this figure is cylindrical and extends to infinity in a direction perpendicular to the paper. This amounts to the lines OP_U and OP_L representing rectangular mirrors and P_U and P_L representing line sources. If a ray emanating from P_L is going to be reflected from OP_U and pass through P then it must be possible to draw a line from the image of P_L to P that intersects OP_U . That is $P_L^I P$ must intersect OP . The point of intersection is P_R and this is the physical point on the mirror struck by the ray emanating from P_L and reflected to pass through P. The same discussion is applicable for the rays emanating from P_U . Because of the symmetry of our antenna we chose to restrict the observation angle, θ , to lie between θ_0 and $\pi/2$. In order for a ray from P_U to be reflected from OP_L and pass through P it is necessary that the image point P_U^I lie on or below the line OP_H . It can be shown that this is possible only if $\theta_0 \geq \pi/6$. Since $\arctan \frac{1}{2} < \pi/6$ we have no reflections from OP_L to consider. We now return to reflections from OP_U . The minimum value of θ for an observation point P' which receives a reflected ray is denoted by θ_1 and it is depicted in figure 15. P' is any point on the extension of the line $P_L^I P_U$ and θ_1 is the angle between OP' and z axis. The explicit expression for θ_1 is given in (44) where r is the length OP' . The maximum value of θ for an observation point P'' which can receive a reflected ray is denoted by θ_2 . P'' is any point on the extension of the line $P_L^I O$ and θ_2 is the angle between OP'' and the z axis. The calculation of θ_1 and θ_2 is straightforward using figure 15; however, the calculation of δ_5 , β_5 , and s_5 is facilitated by modifying figure 15. If we rotate $P_R P$ and OP about the line OP , then we obtain the triangle depicted in figure 16. First we note that $s_5 = P_L P_R + P_R P = P_L P$ and that once we determine

the angle τ , the evaluation of s_5 and ψ becomes elementary. It can be shown that $\tau = \pi + \theta - 3\theta_0$. s_5 is now determined by the law of cosines to yield (43) and ψ given in (42) results from projecting OP to align with OP_L and then applying the definition of cosine. Once ψ is determined, δ_5 and β_5 follow from (41).

It should be mentioned that for certain values of θ_0 it is possible for a ray emanating from either P_U or P_L to get multiply reflected and then pass through P . It can be shown that this is not possible if $\theta_0 < \pi/4$ and this is the situation that was treated in detail in this note.

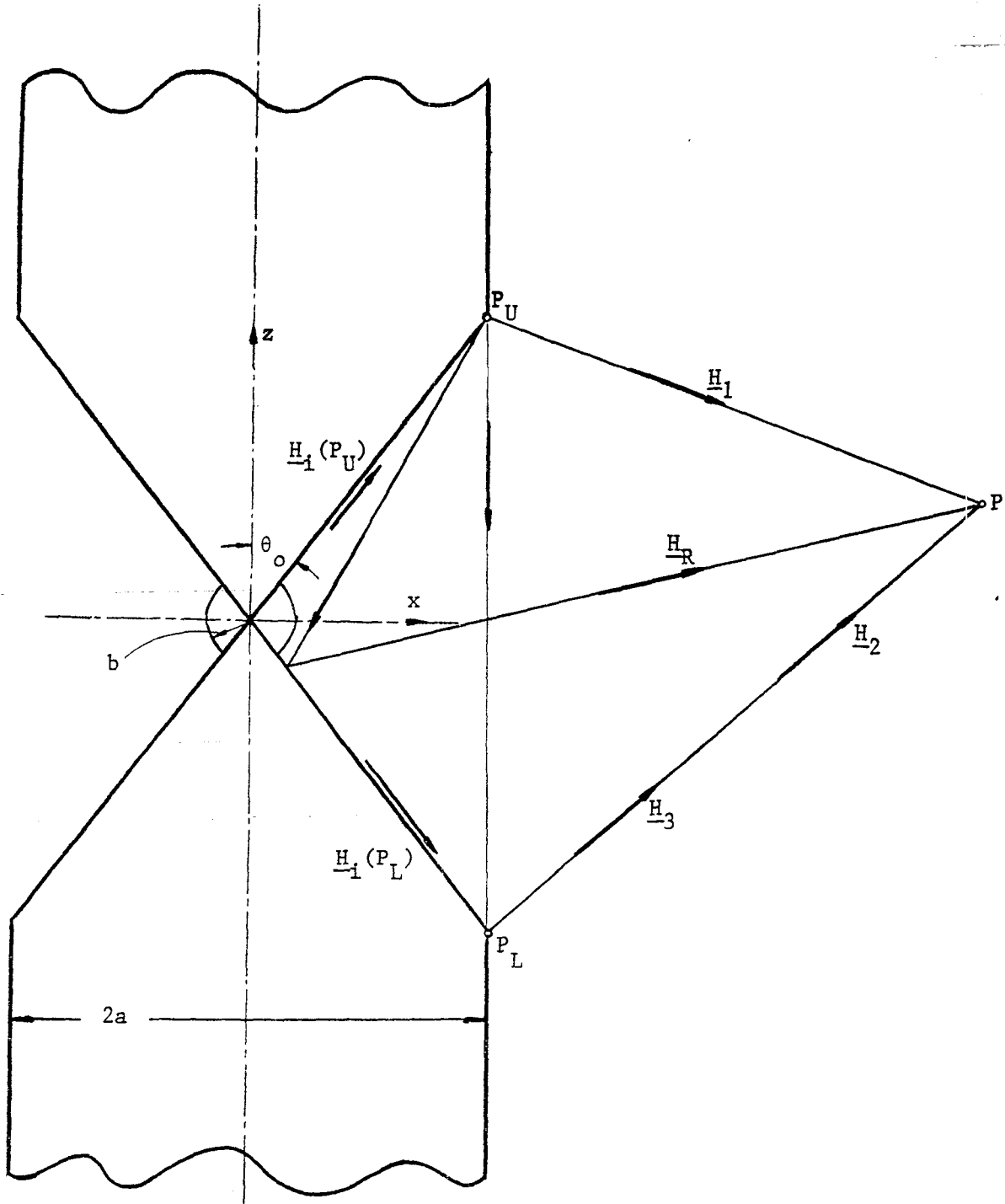


Figure 1. Antenna Geometry.

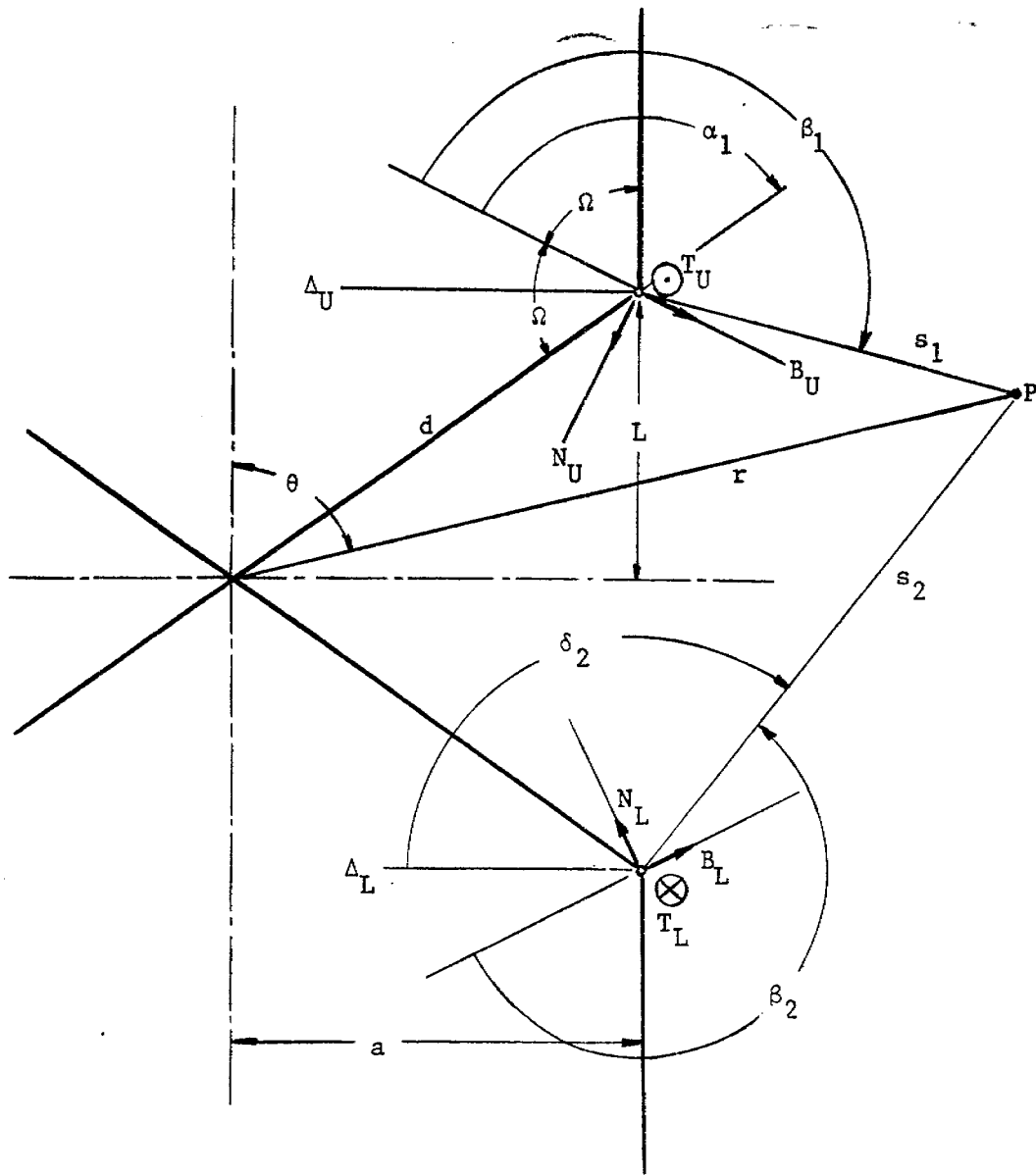


Figure 2. Appropriate Diffraction Coordinate Systems.

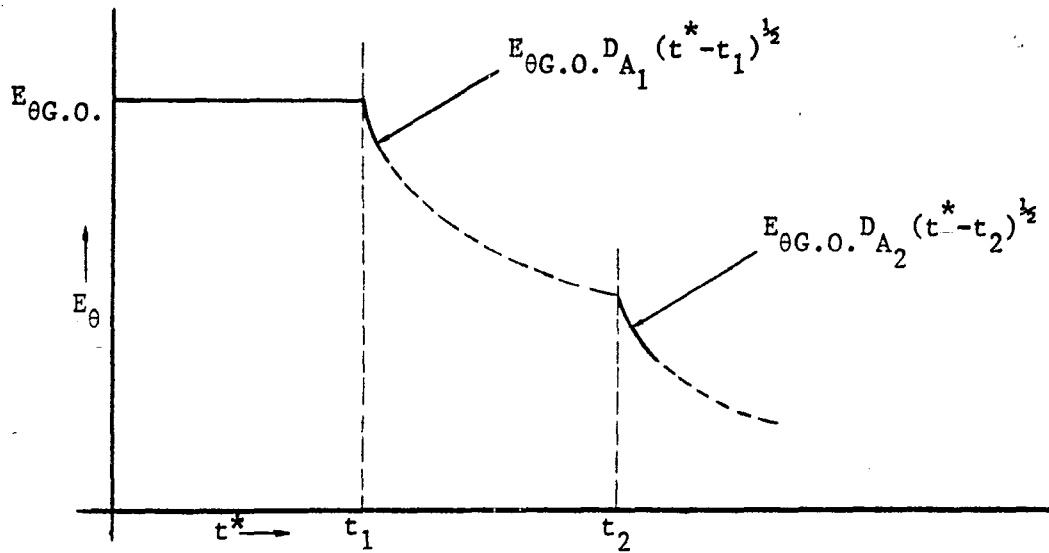


Figure 3a. Schematic Plot of Early Time Asymptotic Breaking Effect for Observation Points in the Illuminated Region.

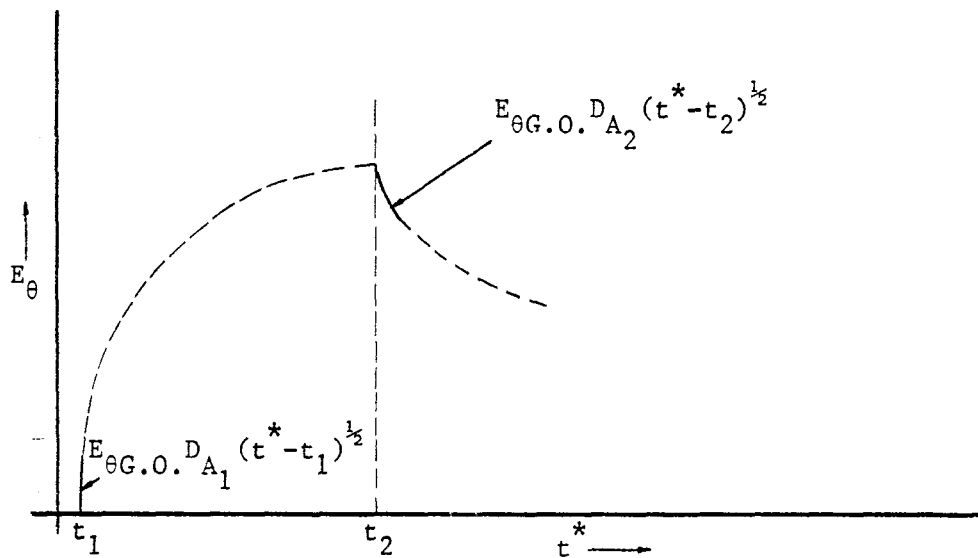


Figure 3b. Schematic Plot of Early Time Asymptotic Breaking Effect for Observation Points in the Diffraction Region.

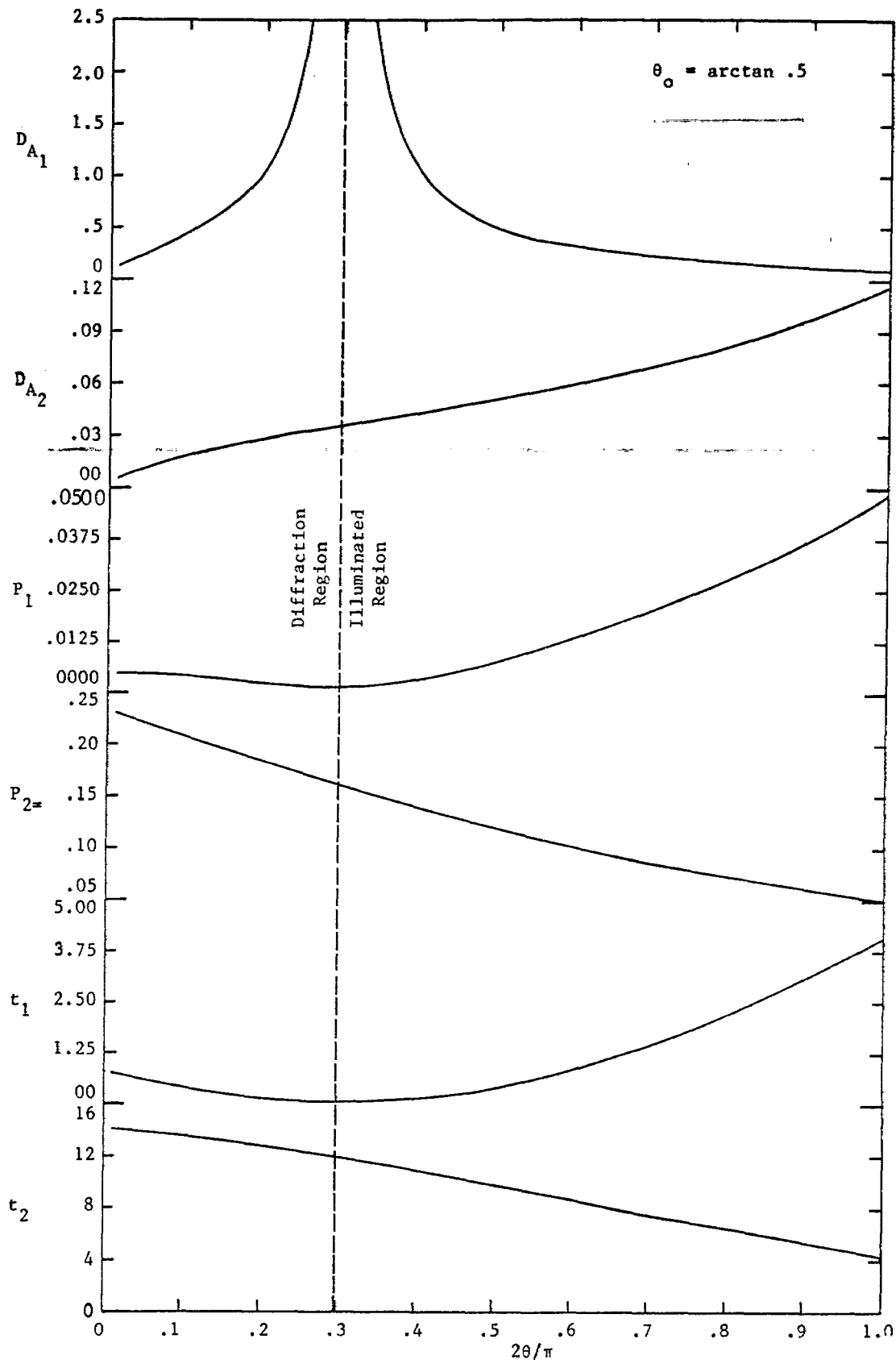


Figure 4.

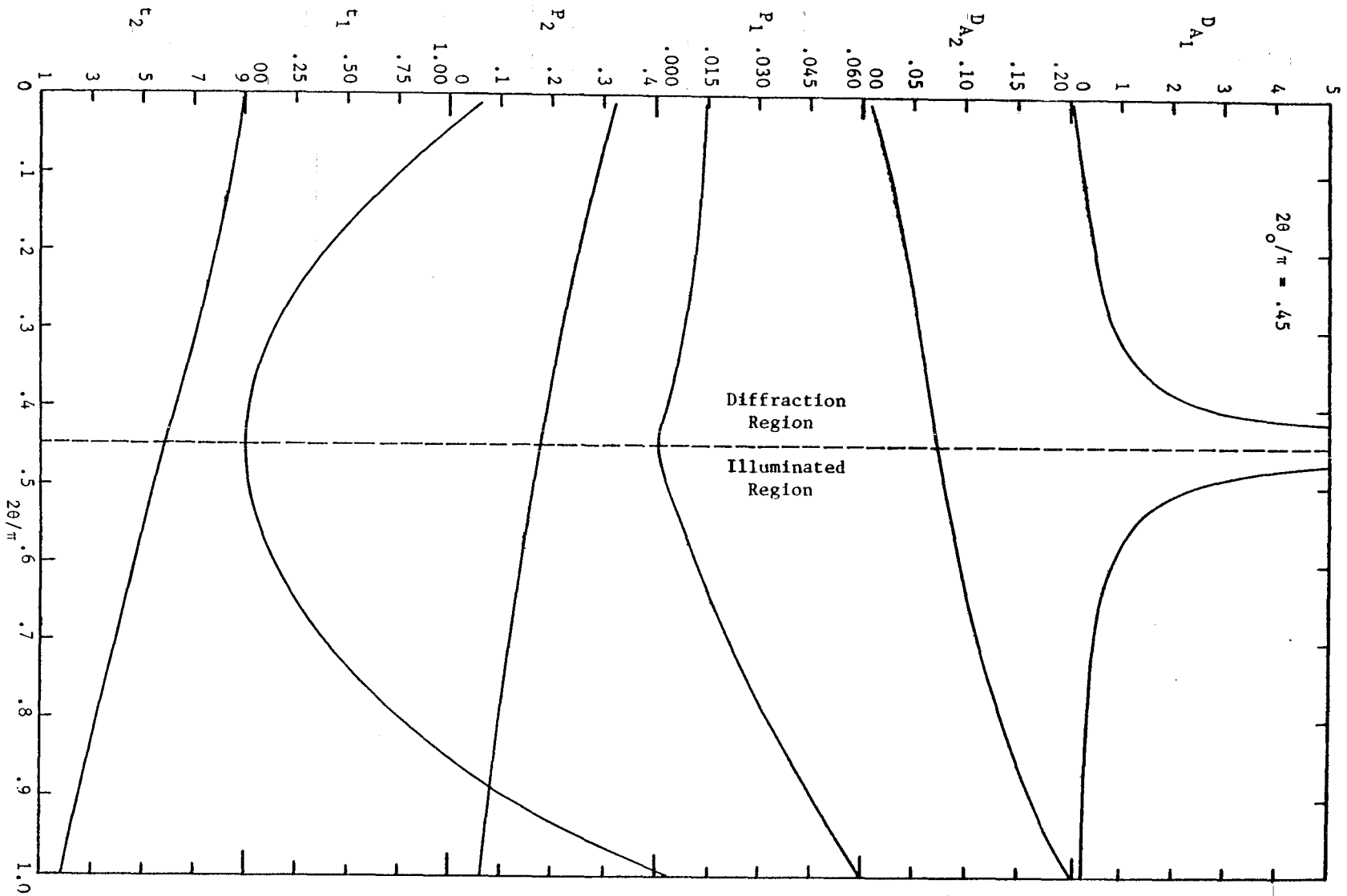


Figure 5.

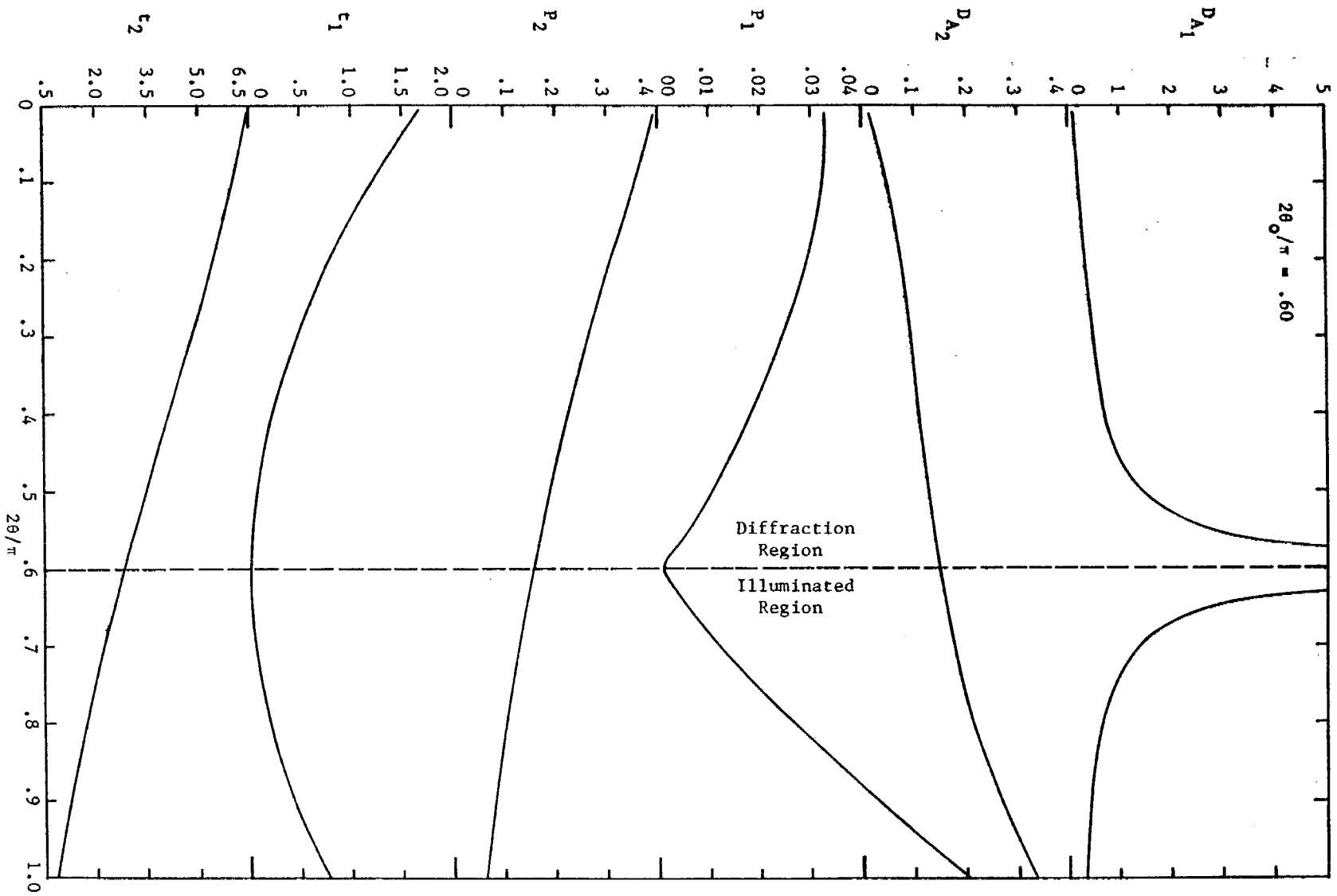


Figure 6.

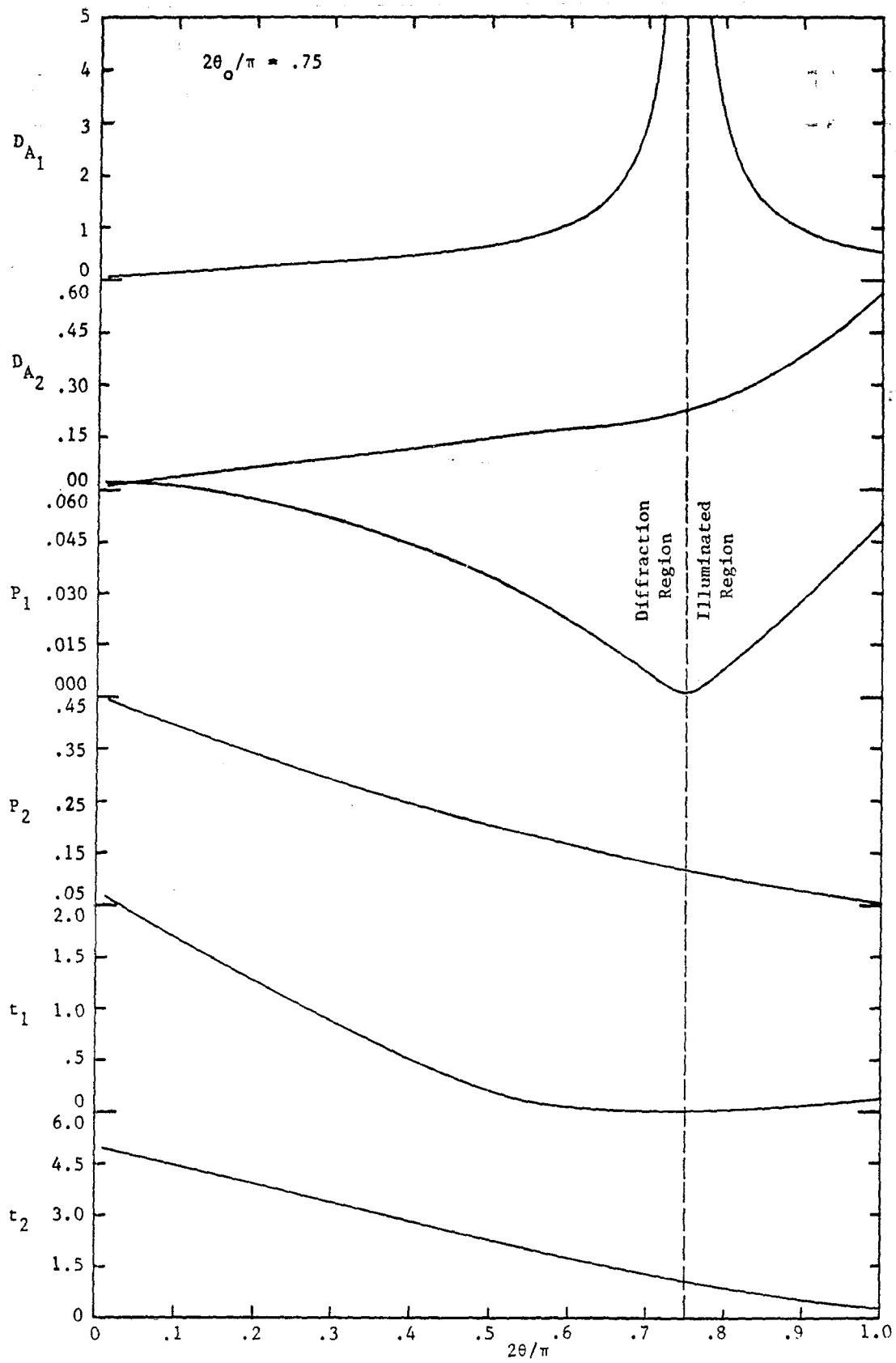


Figure 7.

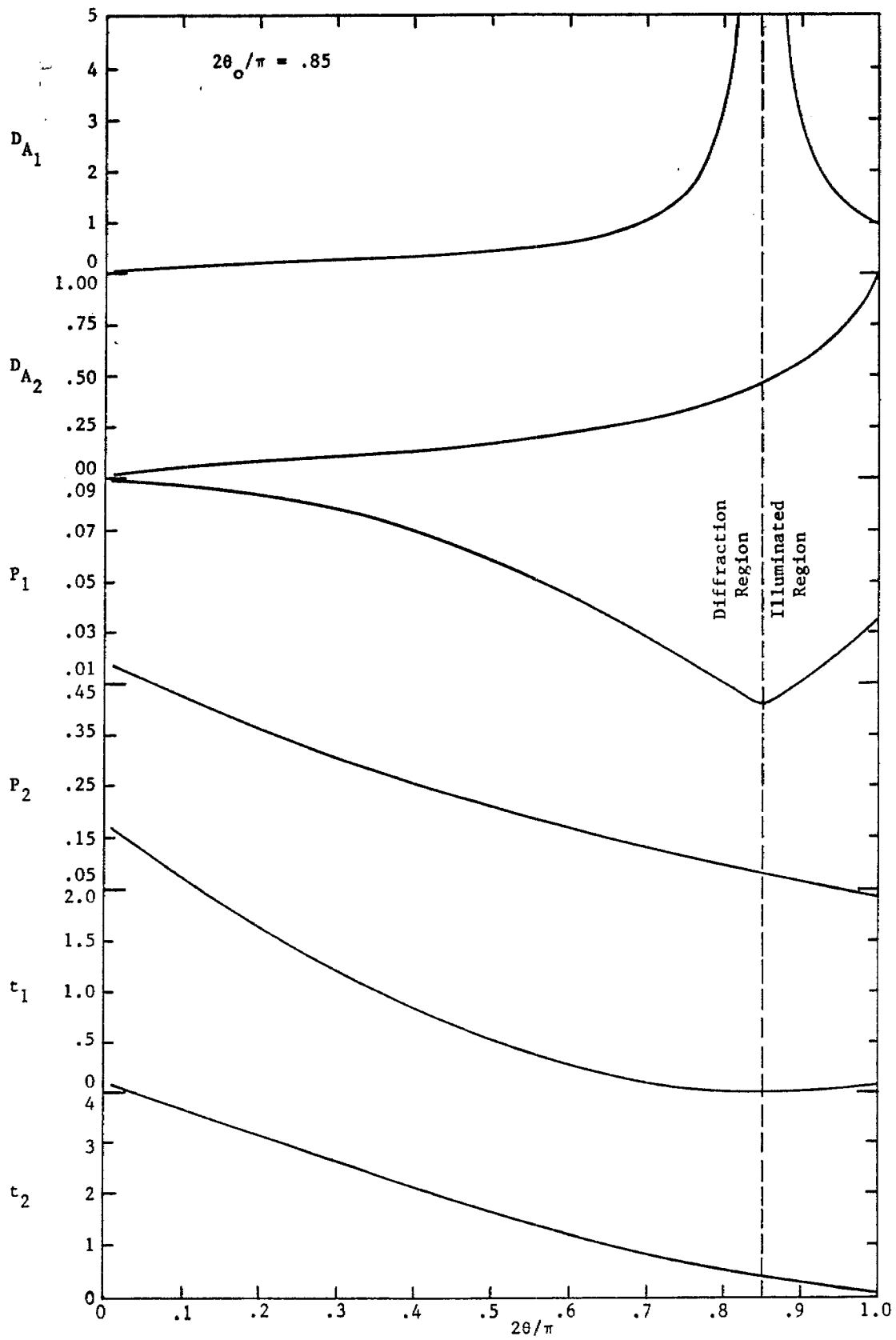


Figure 8.

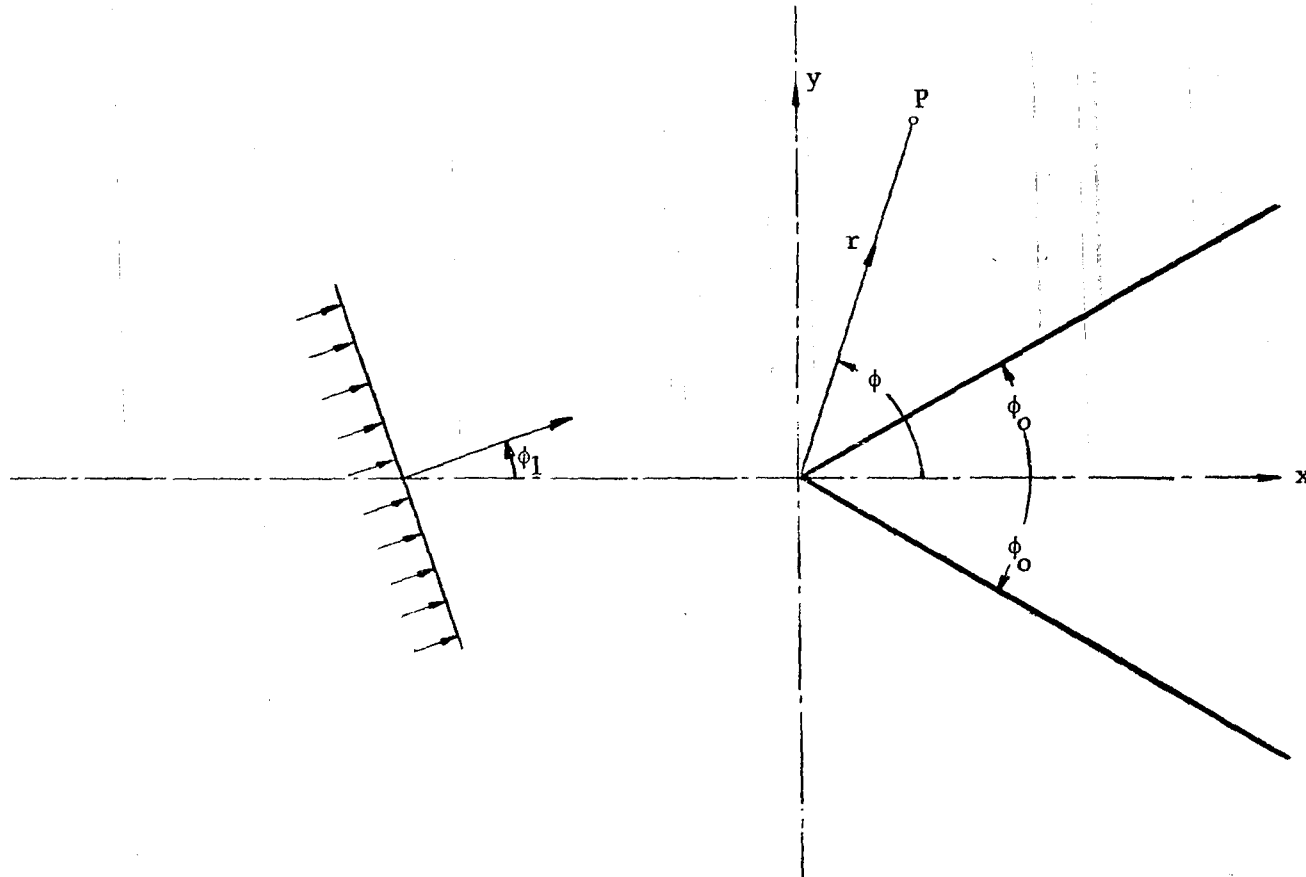


Figure 9. Wedge Scattering Geometry.

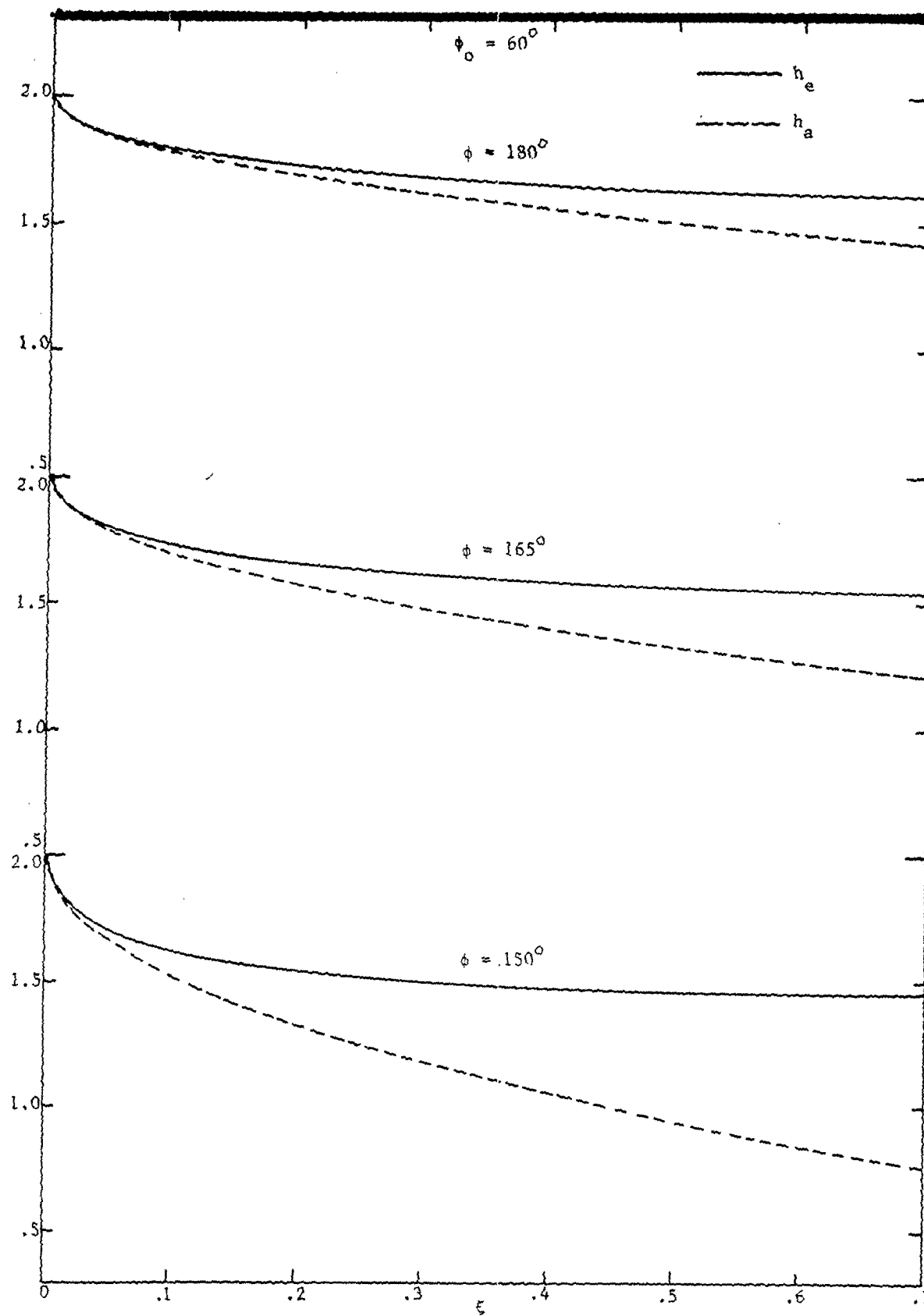


Figure 10.

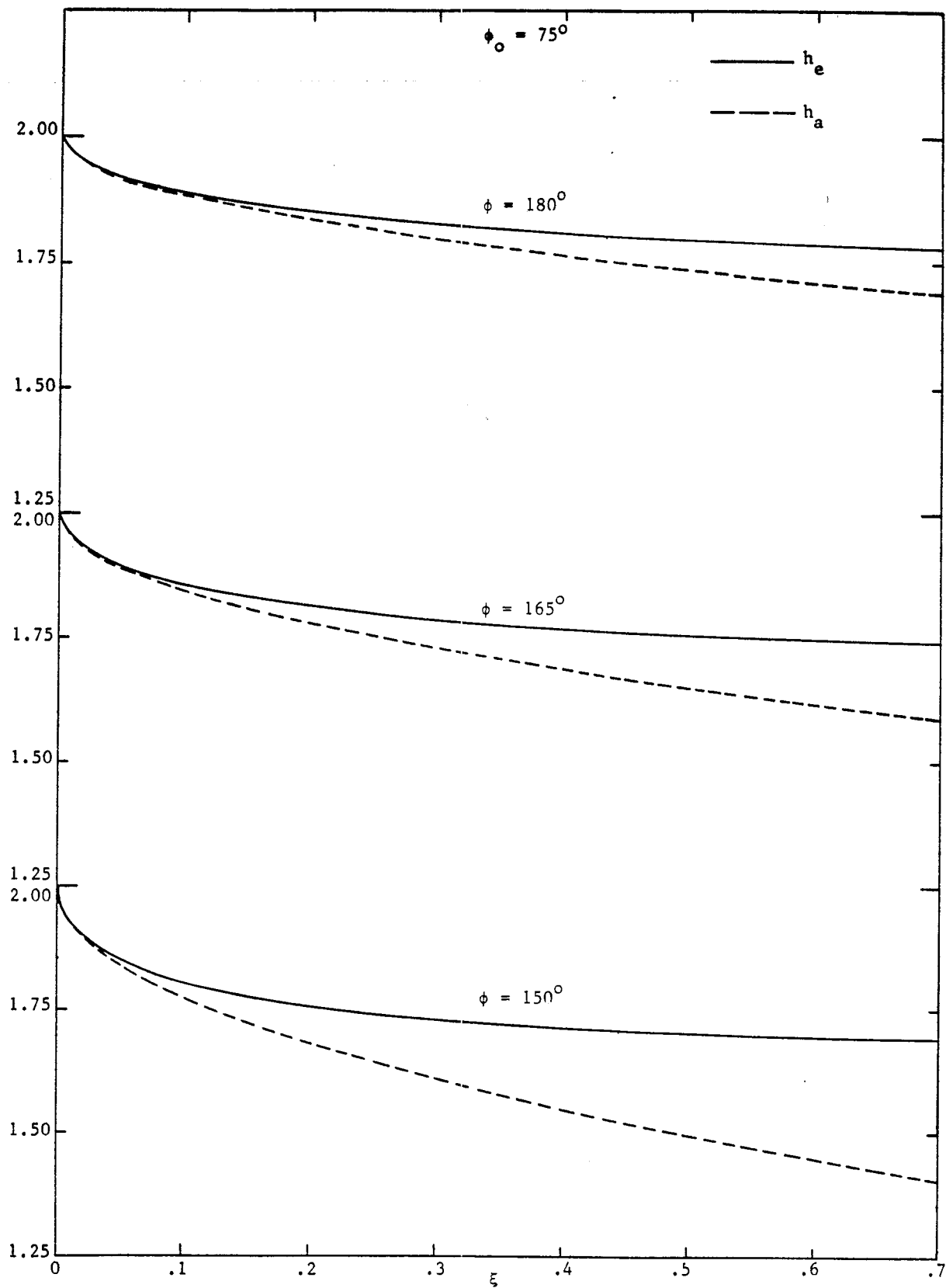


Figure 11.

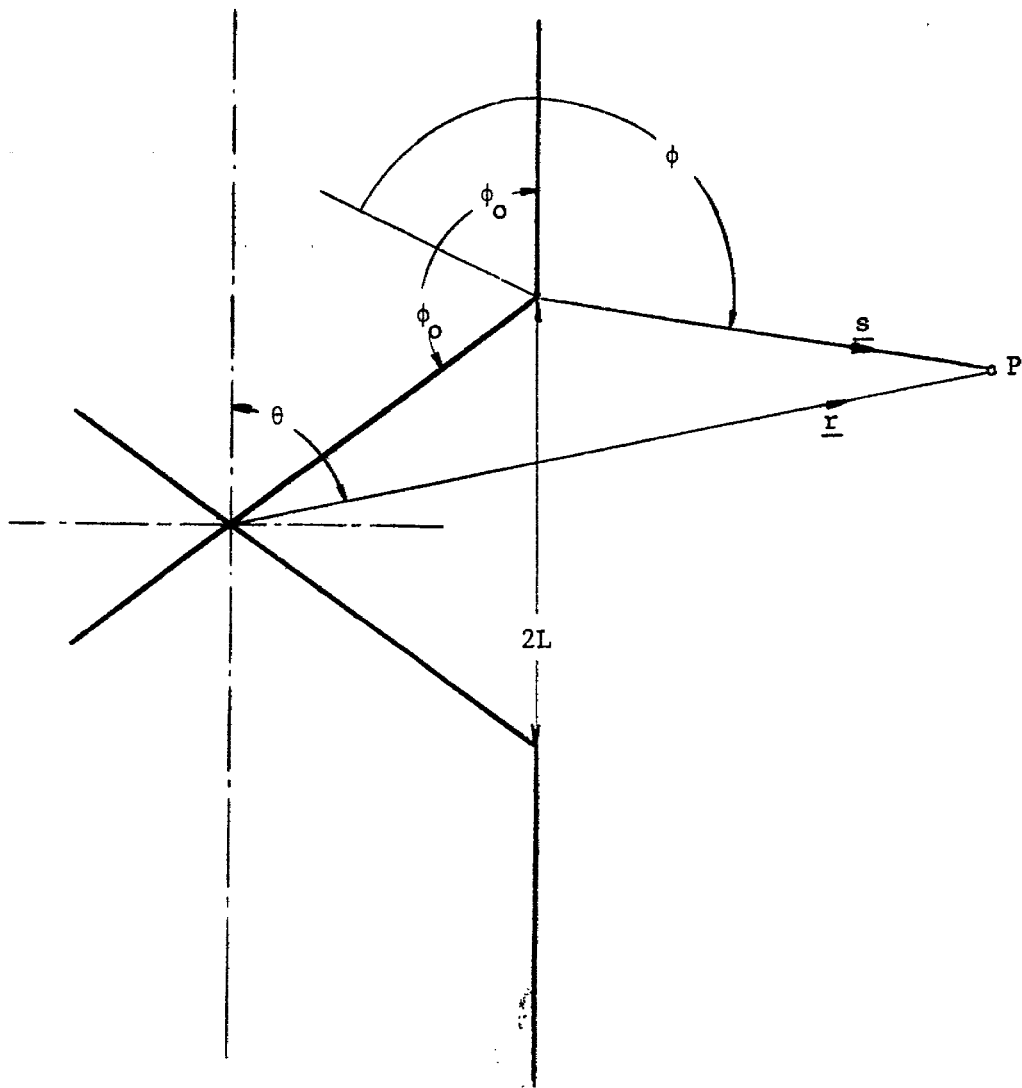


Figure 12. Relationship Between Wedge and Bicone Geometries.

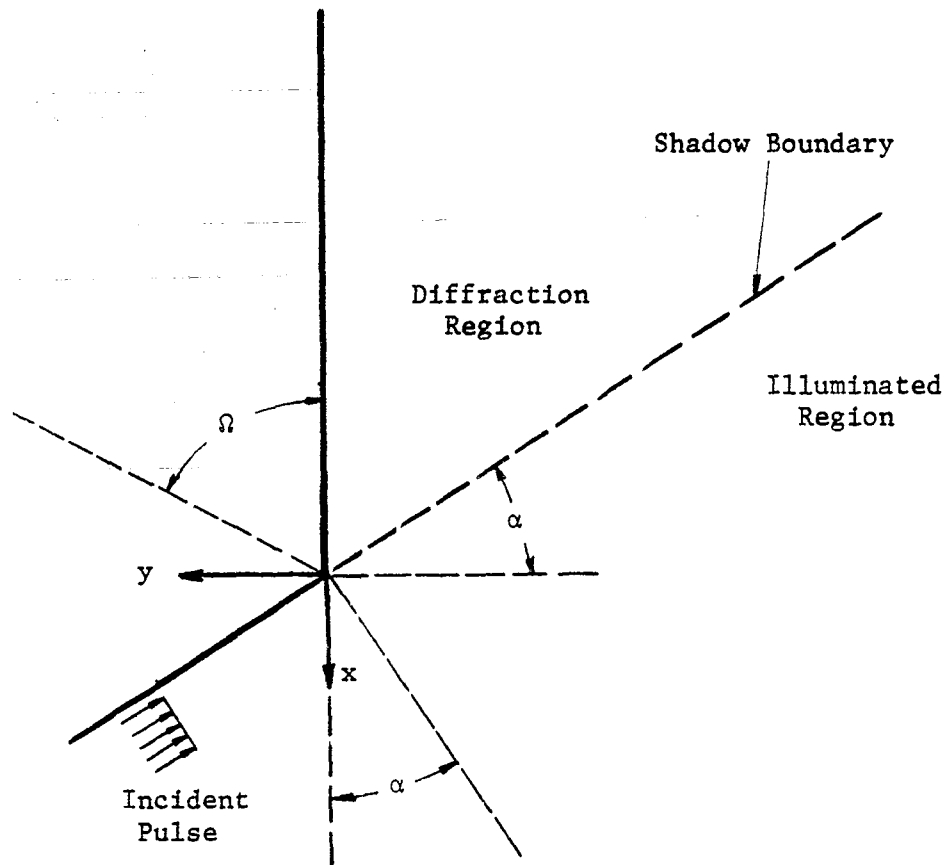


Figure 13. Wedge and Aperture Geometry.

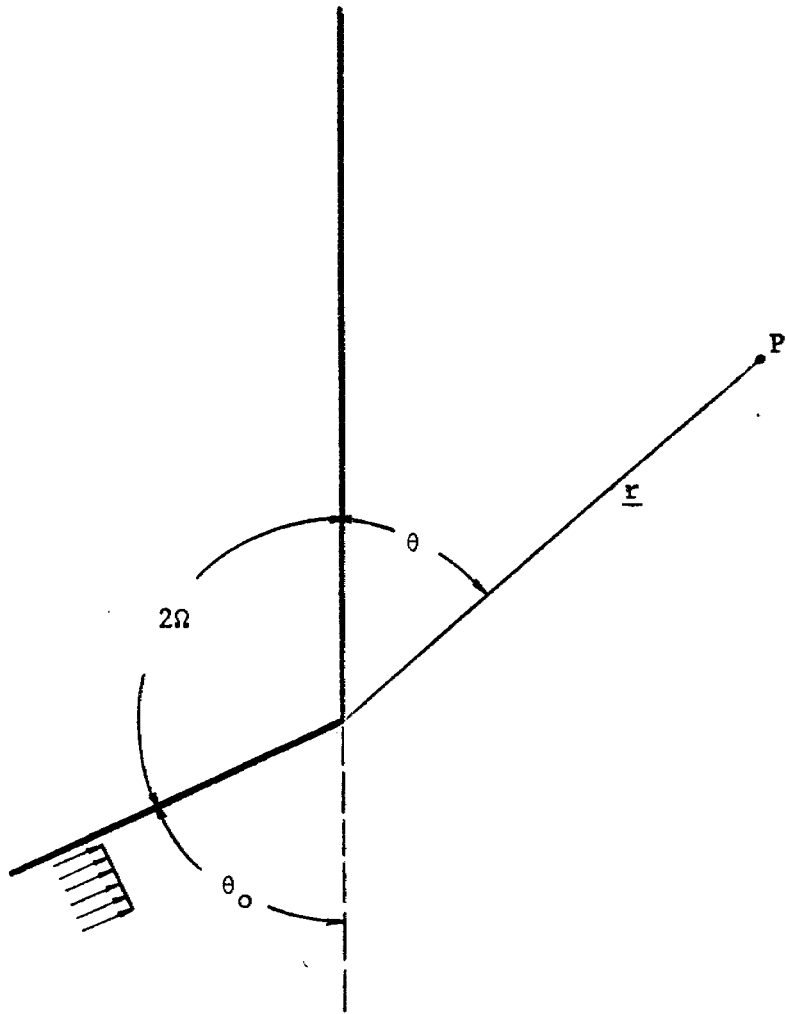


Figure 14. Relationship Between Wedge and Bicone Coordinates.

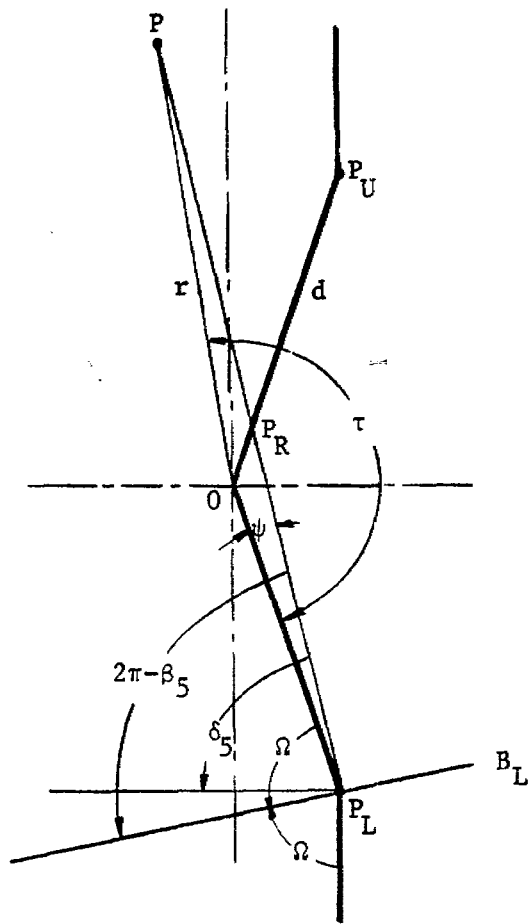


Figure 16. Simplified Geometry for Determination of Reflection Parameters.

Table 1

$a = 1$

$\theta_0 = \arctan .5$

$2\theta/\pi$	D_{A_1}	D_{B_1}	D_{A_2}	D_{B_2}	t_1	t_2
.1	.4693	.4675	.0188	.0232	.3478	13.5260
.2	1.0846	1.0820	.0276	.0332	.0832	12.7727
.3	21.7090	21.7122	.0354	.0416	.0002	11.8885
.5	.4907	.4948	.0513	.0579	.3828	9.8174
.7	.2314	.2362	.0707	.0772	1.4579	7.5153
.9	.1429	.1484	.0982	.1042	3.1205	5.2078
1.0	.1175	.1232	.1175	.1232	4.1231	4.1231
$2\theta_0/\pi = .45$						
.1	.2825	.2786	.0271	.0362	.7569	8.4717
.2	.4722	.4667	.0404	.0520	.3910	7.8197
.3	.8326	.8258	.0524	.0653	.1419	7.1016
.5	2.5168	2.5255	.0780	.0917	.0158	5.5390
.7	.4828	.4931	.1109	.1244	.3910	3.9371
.9	.2518	.2634	.1608	.1735	1.2306	2.4525
1.0	.1983	.2105	.1983	.2105	1.8005	1.8005
$2\theta_0/\pi = .6$						
.1	.2036	.1972	.0352	.0501	1.2076	5.9949
.2	.3142	.3051	.0531	.0720	.7874	5.3972
.3	.4542	.4431	.0698	.0909	.4494	4.7681
.5	1.4196	1.4053	.1070	.1295	.0508	3.4781
.7	1.3899	1.4068	.1586	.1807	.0508	2.2512
.9	.4403	.4594	.2454	.2663	.4494	1.2076
1.0	.3192	.3392	.3192	.3392	.7874	.7874
$2\theta_0/\pi = .75$						
.1	.1582	.1489	.0439	.0657	1.7240	4.4533
.2	.2360	.2227	.0671	.0949	1.2657	3.8937
.3	.3181	.3018	.0897	.1205	.8650	3.3272
.5	.6112	.5902	.1429	.1757	.2748	2.2288
.7	3.0391	3.0144	.2246	.2569	.0111	1.2657
.9	.9724	1.0003	.3893	.4198	.0998	.5320
1.0	.5658	.5950	.5658	.5950	.2748	.2748
$2\theta_0/\pi = .85$						
.1	.1372	.1257	.0505	.0776	2.1177	3.6996
.2	.2020	.1857	.0779	.1125	1.6380	3.1613
.3	.2656	.2456	.1054	.1436	1.2025	2.6296
.5	.4513	.4255	.1737	.2143	.5055	1.6380
.7	1.0563	1.0258	.2892	.3291	.0948	.8219
.9	3.0585	3.0929	.5733	.6109	.0106	.2611
1.0	.9905	1.0266	.9905	1.0266	.0948	.0948

Table 2

a = .5

$\theta_0 = \arctan .5$

$2\theta/\pi$	D_{A_1}	D_{B_1}	D_{A_2}	D_{B_2}	t_1	t_2
.1	.6637	.6611	.0266	.0328	.1739	6.7630
.2	1.5339	1.5302	.0391	.0470	.0416	6.3863
.3	30.7012	30.7057	.0501	.0588	.0001	5.9443
.5	.6940	.6998	.0726	.0818	.1914	4.9087
.7	.3272	.3341	.1000	.1091	.7290	3.7577
.9	.2021	.2099	.1389	.1474	1.5603	2.6039
1.0	.1661	.1743	.1661	.1743	2.0615	2.0615

$2\theta_0/\pi = .45$

.1	.3995	.3939	.0384	.0512	.3784	4.2359
.2	.6679	.6601	.0571	.0735	.1955	3.9099
.3	1.1775	1.1679	.0742	.0924	.0710	3.5508
.5	3.5592	3.5716	.1103	.1297	.0079	2.7695
.7	.6828	.6974	.1569	.1760	.1955	1.9686
.9	.3560	.3725	.2274	.2454	.6153	1.2262
1.0	.2804	.2977	.2804	.2977	.9002	.9002

$2\theta_0/\pi = .6$

.1	.2880	.2789	.0498	.0708	.6038	2.9975
.2	.4444	.4315	.0751	.1019	.3937	2.6986
.3	.6424	.6266	.0987	.1285	.2247	2.3840
.5	2.0076	1.9873	.1514	.1831	.0254	1.7390
.7	1.9656	1.9895	.2242	.2555	.0254	1.1256
.9	.6227	.6497	.3470	.3766	.2247	.6038
1.0	.4514	.4798	.4514	.4798	.3937	.3937

$2\theta_0/\pi = .75$

.1	.2238	.2105	.0621	.0929	.8620	2.2267
.2	.3337	.3150	.0950	.1342	.6328	1.9469
.3	.4498	.4269	.1268	.1704	.4325	1.6636
.5	.8643	.8347	.2021	.2485	.1374	1.1144
.7	4.2980	4.2630	.3177	.3633	.0056	.6328
.9	1.3751	1.4146	.5505	.5937	.0499	.2660
1.0	.8001	.8415	.8001	.8415	.1374	.1374

$2\theta_0/\pi = .85$

.1	.1941	.1777	.0714	.1098	1.0588	1.8498
.2	.2857	.2626	.1102	.1591	.8190	1.5806
.3	.3756	.3473	.1491	.2031	.6013	1.3148
.5	.6382	.6017	.2456	.3030	.2528	.8190
.7	1.4938	1.4507	.4090	.4654	.0474	.4110
.9	4.3253	4.3740	.8108	.8640	.0053	.1306
1.0	1.4008	1.4519	1.4008	1.4519	.0474	.0474

Table 3

$a = 2$

$\theta_0 = \arctan .5$

$2\theta/\pi$	D_{A_1}	D_{B_1}	D_{A_2}	D_{B_2}	t_1	t_2
.1	.3318	.3306	.0133	.0164	.6955	27.0521
.2	.7669	.7651	.0200	.0135	.1664	25.5454
.3	15.3506	15.3528	.0251	.0294	.0004	23.7770
.5	.3470	.3499	.0363	.0409	.7655	19.6347
.7	.1636	.1670	.0500	.0546	2.9159	15.0307
.9	.1011	.1050	.0694	.0737	6.2410	10.4155
1.0	.0831	.0871	.0831	.0871	8.2461	8.2461
$2\theta_0/\pi = .45$						
.1	.1997	.1970	.0192	.0256	1.5137	16.9435
.2	.3339	.3300	.0286	.0368	.7819	15.6394
.3	.5887	.5840	.0371	.0462	.2838	14.2032
.5	1.7796	1.7858	.0551	.0649	.0317	11.0782
.7	.3414	.3487	.0784	.0880	.7819	7.8742
.9	.1780	.1863	.1137	.1227	2.4612	4.9050
1.0	.1402	.1489	.1402	.1489	3.6009	3.6009
$2\theta_0/\pi = .6$						
.1	.1440	.1395	.0249	.0354	2.4152	11.9898
.2	.2222	.2158	.0375	.0509	1.5749	10.7943
.3	.3212	.3133	.0494	.0642	.8988	9.5361
.5	1.0038	.9937	.0757	.0916	.1015	6.9562
.7	.9828	.9948	.1121	.1278	.1015	4.5025
.9	.3113	.3249	.1735	.1883	.8988	2.4152
1.0	.2257	.2399	.2257	.2379	1.5749	1.5749
$2\theta_0/\pi = .75$						
.1	.1119	.1053	.0311	.0465	3.4480	8.9066
.2	.1669	.1575	.0475	.0671	2.5313	7.7875
.3	.2249	.2134	.0634	.0852	1.7301	5.6544
.5	.4322	.4174	.1010	.1242	.5497	4.4576
.7	2.1490	2.1315	.1588	.1817	.0223	2.5313
.9	.6876	.7073	.2753	.2968	.1995	1.0641
1.0	.4001	.4208	.4001	.4208	.5497	.5497
$2\theta_0/\pi = .85$						
.1	.0970	.0889	.0357	.0549	4.2353	7.3991
.2	.1428	.1313	.0551	.0795	3.2761	6.3225
.3	.1878	.1737	.0745	.1015	2.4051	5.2592
.5	.3191	.3009	.1228	.1515	1.0110	3.2761
.7	.7469	.7253	.2045	.2327	.1896	1.6438
.9	2.1627	2.1870	.4054	.4320	.0211	.5222
1.0	.7004	.7260	.7004	.7260	.1896	.1896

Table 4

$$a = 5$$

$$\theta_0 = \arctan .5$$

$2\theta/\pi$	D_{A_1}	D_{B_1}	D_{A_2}	D_{B_2}	t_1	t_2
.1	.2099	.2091	.0084	.0104	1.7388	67.6302
.2	.4851	.4839	.0124	.0148	.4159	63.8635
.3	9.7086	9.7100	.0158	.0186	.0011	59.4425
.5	.2195	.2213	.0230	.0259	1.9138	49.0868
.7	.1035	.1056	.0316	.0345	7.2897	37.5766
.9	.0639	.0664	.0439	.0466	15.6026	26.0388
1.0	.0525	.0551	.0525	.0551	20.6154	20.6154

$$2\theta_0/\pi = .45$$

.1	.1263	.1246	.0121	.0162	3.7843	42.3587
.2	.2112	.2087	.0181	.0233	1.9548	39.0986
.3	.3723	.3693	.0235	.0292	.7096	35.5081
.5	1.1255	1.1294	.0349	.0410	.0792	27.6954
.7	.2159	.2205	.0496	.0556	1.9548	19.6855
.9	.1126	.1178	.0719	.0776	6.1529	12.2625
1.0	.0887	.0941	.0887	.0941	9.0024	9.0024

$$2\theta_0/\pi = .6$$

.1	.0911	.0882	.0158	.0224	6.0381	29.9745
.2	.1405	.1365	.0237	.0322	3.9372	26.9859
.3	.2031	.1982	.0312	.0406	2.2469	23.8403
.5	.6349	.6285	.0479	.0579	.2538	17.3904
.7	.6216	.6291	.0709	.0808	.2538	11.2562
.9	.1969	.2055	.1097	.1191	2.2469	6.0381
1.0	.1427	.1517	.1427	.1517	3.9372	3.9372

$$2\theta_0/\pi = .75$$

.1	.0708	.0666	.0197	.0294	8.6200	22.2666
.2	.1055	.0996	.0300	.0424	6.3283	19.4687
.3	.1422	.1350	.0401	.0539	4.3252	16.6360
.5	.2733	.2640	.0639	.0786	1.3742	11.1440
.7	1.3591	1.3481	.1005	.1149	.0556	6.3283
.9	.4349	.4473	.1741	.1877	.4988	2.6602
1.0	.2530	.2661	.2530	.2661	1.3742	1.3742

$$2\theta_0/\pi = .85$$

.1	.0614	.0562	.0226	.0347	10.5883	18.4978
.2	.0903	.0830	.0349	.0503	8.1901	15.8064
.3	.1188	.1098	.0471	.0642	6.0127	13.1480
.5	.2018	.1903	.0777	.0958	2.5275	8.1901
.7	.4724	.4587	.1293	.1472	.4739	4.1095
.9	1.3678	1.3832	.2564	.2732	.0529	1.3056
1.0	.4430	.4591	.4430	.4591	.4739	.4739

Table 5

$2\theta/\pi$	$\theta_o = \arctan .5$		$2\theta_o/\pi = .45$		$2\theta_o/\pi = .6$		$2\theta_o/\pi = .75$		$2\theta_o/\pi = .85$	
	P_1	P_2	P_1	P_2	P_1	P_2	P_1	P_2	P_1	P_2
.1	.0039	.2082	.0139	.2865	.0320	.3478	.0610	.3972	.0878	.4240
.2	.0024	.1830	.0117	.2510	.0293	.3029	.0578	.3426	.0843	.3627
.3	.0001	.1601	.0081	.2185	.0248	.2618	.0524	.2928	.0783	.3067
.5	.0083	.1200	.0035	.1618	.0102	.1900	.0349	.2059	.0589	.2093
.7	.0208	.0868	.0211	.1148	.0121	.1304	.0082	.1341	.0293	.1290
.9	.0378	.0596	.0452	.0762	.0425	.0817	.0283	.0753	.0112	.0635
1.0	.0480	.0480	.0598	.0598	.0610	.0610	.0504	.0504	.0358	.0358

Acknowledgement

We thank Dr. C. E. Baum for his helpful comments and Dr. K. S. H. Lee for his continued interest.

References

1. Baum, C. E., "Design of a Pulse-Radiating Dipole Antenna as Related to High-Frequency and Low-Frequency Limits," *Sensor and Simulation Note* 69, January 1969.
2. Keller, J. B., "Diffraction by an Aperture," *J. Appl. Phys.*, 28, p. 426, 1957.
3. Keller, J. B., "Geometrical Theory of Diffraction," *J. Opt. Soc. Am.*, 52, p. 116, 1962.
4. Barnes, P. R., "Pulse Radiation by an Infinitely Long, Perfectly Conducting, Cylindrical Antenna in Free Space Excited by a Finite Cylindrical Distributed Source Specified by the Tangential Electric Field Associated with a Biconical Antenna," *Sensor and Simulation Note* 110, July 1970.
5. Senior, T. B. A. and P. L. E. Uslenghi, "High-Frequency Backscattering from a Finite Cone," *Radio Sci.*, 6, p. 393, 1971.
6. Baum, C. E., "The Diffraction of an Electromagnetic Plane Wave at a Bend in a Perfectly Conducting Planar Sheet," *Sensor and Simulation Note* 47, August 1967.
7. Keller, J. B. and A. Blank, "Diffraction and Reflection of Pulses by Wedges and Corners," *Comm. Pure and Appl. Math.*, 4, p. 75, 1951.
8. Bowman, J. J., T. B. A. Senior, and P. L. E. Uslenghi, Electromagnetic and Acoustic Scattering by Simple Shapes, John Wiley and Sons, Inc., New York, p. 262, 1969.
9. Baum, C. E. "A Simplified Two-Dimensional Model for the Fields Above the Distributed-Source Surface Transmission Line," *Sensor and Simulation Note* 66, December 1968.